The Decomposition of Deformation: new metrics to enhance shape analysis in medical imaging.

Valerio Varano[a,*], Paolo Piras[b,c], Stefano Gabriele[a], Luciano Teresi[d], Paola Nardinocchi[c], Ian L. Dryden[e], Concetta Torromeo[b], Paolo E. Puddu[b]

[a] *Dipartimento di Architettura, LaMS Modeling & Simulation Lab, Università Roma Tre, Rome, Italy.*
[b] *Dipartimento di Scienze Cardiovascolari, Respiratorie, Nefrologiche, Anestesiologiche e Geriatriche, Sapienza, Università di Roma, Rome, Italy*
[c] *Dipartimento di Ingegneria Strutturale e Geotecnica, Sapienza, Università di Roma, Rome, Italy.*
[d] *Dipartimento di Matematica e Fisica, LaMS Modeling & Simulation Lab, Università Roma Tre, Rome, Italy.*
[e] *School of Mathematical Sciences, University of Nottingham, Nottingham, UK.*

Abstract

In landmarks-based Shape Analysis size is measured, in most cases, with Centroid Size. Changes in shape are decomposed in affine and non affine components. Furthermore the non affine component can be in turn decomposed in a series of local deformations (partial warps). If the extent of deformation between two shapes is small, the difference between centroid size and m-Volume increment is barely appreciable. In medical imaging applied to soft tissues bodies can undergo very large deformations, involving large changes in size. The cardiac example, analyzed in the present paper, shows changes in m-Volume that can reach the 60%. We show here that standard Geometric Morphometrics tools (landmarks, Thin Plate Spline, and related decomposition of the deformation) can be generalized to better describe the very large deformations of biological tissues, without losing a synthetic description. In particular, the classical decomposition of the space tangent to the shape space in affine and non affine components is enriched to include also the change in size, in order to give a complete description of the tangent space to the size-and-shape space. The proposed generalization is formulated by means of a new Riemannian metric describing the change in size as change in m-Volume rather than change in Centroid Size. This leads to a redefinition of some aspects of the Kendall's size-and-shape space without losing Kendall's original formulation. This new formulation is discussed by means of simulated examples using 2D and 3D platonic shapes as well as a real example from clinical 3D echocardiographic data. We demonstrate that our decomposition based approaches discriminate very effectively healthy subjects from patients affected by Hypertrophic Cardiomyopathy.

Keywords: Geometric Morphometrics, Decomposition of Deformation, Riemannian Metrics, Size and Shape, Left Ventricle Deformation

*Corresponding Author
Email address: valerio.varano@uniroma3.it (Valerio Varano)

1. Introduction

Medical image analysis experienced, in the last two decades, a significant boost in both shape recognition from medical images and analysis of related geometric data. In particular, 2D and 3D Speckle Tracking Echocardiography (2D and 3D STE), CT-scan and Magnetic Resonance (MR) represented the most used technologies, albeit not unique, in order to extract anatomical shapes from medical images to be analyzed and evaluated in terms of form, function and, ultimately, physiology. Shapes are identified by points (=landmarks) in 2D/3D space. These landmarks can be considered (with a certain degree of approximation) anatomically homologous, or not, between different subjects. In the former case anatomical homology allows the possibility to treat landmarks with the standard Geometric Morphometrics (GM) toolkit (see below). Without homology' assumption several strategies have been developed in order to perform shape matching basing on a plethora of algorithms (Bronstein A. and Bronstein M., 2013) whose review is not the scope of the present paper. In the last years the emerging disciplines of Diffeomorphometry and the related Functional Anatomy apply to replace classic GM through the use of diffeomorphisms, more suitable to describe soft tissues changes (Miller M. I.and Qiu A., 2009; Miller et al., 2013, 2014, 2015). On the other hand, these descriptions are very sophisticated but do not incorporate in their formulation some synthetic properties of the decomposition of deformation in some significant aspects. In this paper we focus on shapes represented by landmarks that are considered anatomically homologous in different configurations. Very often, in medical applications, the goal of shape analysis is not the assessment of differences between shapes; rather, the main aim is to find differences between deformations. This distinction is crucial [3] and inevitably leads to the definition and quantification of deformation occurring between two shapes, e.g. a source and a target. Thus, before entering the clinical and physiological interpretation of the primary medical datum, it is compelling to understand how the total observed deformation can be decomposed in its main components, the one related to pure size, that related to a global affine deformation and that representing a non affine transformation. GM and differential geometry' tools can be combined in different ways in order to answer differently to the same question. Thus, in advance of presenting our clinical example, related to 3D STE data of healthy subjects and of patients affected by Hypertrophic Cardiomyopathy (HCM), we necessarily must present the techniques used to decompose the deformation with the help of explicit/controlled simulated examples. After that, the return to the real clinical case will be eased by the augmented awareness of how and why a deformation is decomposed.

First of all we will show how decomposing the deformation can help in describing the mechanical behaviour of the myocardium, highlighting the different mechanical role of the two layers (Evangelista et al., 2015). Second, we prove the ability of the threefold decomposition in discriminating the HCM pathology from Control subjects.

HCM is one the most common genetically determined cardiac disease. It results from functional impairments of myocardial proteins and about 13 genes have been identified as responsibles of pathology. This causes a muscular fiber disarray with a consequent dysfunctional contraction, an augmented left ventricular pressure during filling as well as a huge left atrium hyperdilation. Left ventricle dynamics in HCM presents an increased duration of LV twist consequent to the inverse relationship of longitudinal strain rate and twist rate. This is viewed as a compensation to preserve ejection fraction (= systolic function). However, the increased duration of systolic twist induces an untwisting delay, with elevated LV early diastolic pressures, reduced transmitral pressure gradient and impaired LV early diastolic filling.Albeit the diagnosis can be easily done using classic Echocardiography, studying in detail the mechanical behaviour of epicardium and endocardium would be of great help in understanding how and where the pathology affects the left ventricular anatomy. For example, it can be hypothesized that the muscular fiber's disarray could be at the base of an augmented non affine component of deformation due to the irregularity of fiber's orientation.

In (Rohlf, F.J. and Bookstein, F.L. , 2003) it was added to the existing method proposed in (Bookstein, 1996a) other two methods for computing the affine component in a transformation: i) the complement of the space of pure bending shape variation; ii) the regression method. Relatively to (Bookstein, 1996a) these two methods do not require the reference configuration to be aligned to its principal axes. While the former implies the computation of the bending energy matrix, the latter does not and can be easily implemented using the computation of the pseudoinverse matrix in a linear system relating the source and the target configurations. This solution is the same as the least squares estimator when we wish to estimate the affine transformation between a source and a target. In (Dryden, I.L., Mardia, K.V., 2016) further details about this are given (see Equation (12.2) and Subsection (12.2.2) of the book). These approaches were presented in the shape space, thus after scaling shapes at unit size. We present our decomposition strategy in the size and shape space thus taking in account the contribution of size difference between source and target.

Moreover, we do this by optionally computing the affine component using Thin Plate Spline (TPS) or the pseudoinverse strategy (that is equivalent to the 'regression' method in (Rohlf, F.J. and Bookstein, F.L. , 2003)). It is worth noting that the 'complement of the space of pure bending shape variation' method proposed by (Rohlf, F.J. and Bookstein, F.L. , 2003) looks for the pure affine component after computing the bending energy matrix thus using the TPS paradigm. However, they do not use the affine component of the TPS formulation as it is not orthogonal to the non affine one (see below). Instead, they compute the orthogonal complement to the non affine part.

Our procedure furnishes both the magnitude and percentages relative to the whole deformation

of pure homothetic, deviatoric and non affine components. These components belong to different subspaces depicted in Fig.1.

The deviatoric component represents the affine non homothetic component, often called simply 'affine' in classic Geometric Morphometrics given that very often it is referred to transformations in the shape space. On the basis of this we will refer, from now on, to the non affine component as not having any homothetic component.

Deviatoric plus non affine component represent the global non homothetic component. It is important to note that all components depicted in Fig.1 should be orthogonal between each other. This can be verified using formulas defining the angle between two deformation vectors. The angle between deviatoric and non affine components deserves particular attention: in fact it is easily verifiable that, when using TPS approach they are not orthogonal. This is due to the following fact. The landmark-wise representation of the TPS formulation (in (Dryden, I.L., Mardia, K.V., 1998), eq. 10.6) is

$$\psi(x) = c + A\,x + W^T\,s(x)\,, \quad x \in \mathcal{E}^m\,,$$

being $\mathcal{E}^m$ the m-dimensional Euclidean space. Using the shape-wise representation, where a configuration X is defined in the $\mathcal{C}_m^k$ configuration space (with k the number of landmarks), we have

$$\psi(X) = l_k\,c^T + X\,A^T + S\,W\,, \quad X \in\ \mathcal{C}_m^k\,, \quad S_{ij} = \sigma(x_i - x_j)\,, \tag{1.1}$$

where

$$\sigma(h) = \begin{cases} ||h||^2 \log(||h||^2) & \text{if } ||h|| > 0; \\ 0 & \text{if } ||h|| = 0. \end{cases} \qquad \text{for } m = 2$$

$$\sigma(h) = \begin{cases} -||h|| & \text{if } ||h|| > 0; \\ 0 & \text{if } ||h|| = 0. \end{cases} \qquad \text{for } m = 3$$

we have $X\,A^T \perp W$, but $X\,A^T$ is not orthogonal to $S\,W$. On the opposite, when using the pseudoinverse strategy the affine and non affine components are orthogonal.

We propose three methods to decompose the deformation in spherical, deviatoric (i.e. affine non-spherical) and non affine components: 1) The "Fully Euclidean" based on the Pseudoinverse. We use the term "Fully Euclidean" relatively to the decomposition per se and not to the preliminary alignment procedure. Advantages: the components are orthogonal with respect to the Euclidean metric. 2) A new method "GPp" based on the pseudoinverse but using as metric, in the affine subspace, the metric of GL(m) i.e. $Tr(A^T A)$ where A is the linear transformation obtained with the pseudoinverse. In the non affine subspace the metric is still Euclidean. Here the spherical part is related to the change in m-Volume instead of Centroid Size. 3) A method "TPSs" based on the metric introduced in (Varano et al., 2017) called TPS metric. Also in this case the spherical component is related to the change in m-Volume. The advantage of this approach is that the affine

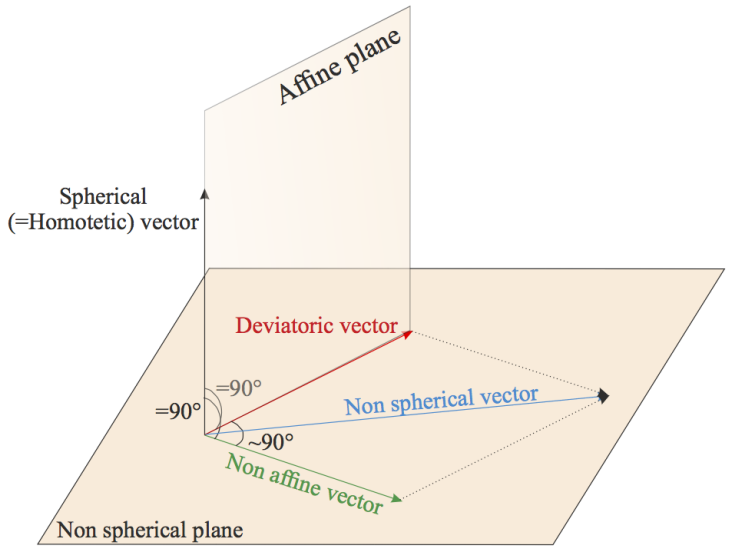

Figure 1: The orthogonal subspaces identified by their corresponding vectors. Spherical, deviatoric and non affine components should be orthogonal under a given decomposition metric.

and non affine components emerge from the TPS decomposition, thus allowing an interpolation with grids. Using this metric XA^T and SW are orthogonal.

Each of these criteria is used to decompose deformations in simulated cases:

1) family of rectangles with different aspect ratios but fixed Centroid Size (CS),

2) family of rectangles with different aspect ratios but fixed m-Volume,

3) 2D bilinear deformations (bending) of a rectangle in a family of trapezoids,

4) 3D bilinear deformations of a parallelepiped.

The same is done using real clinical data coming from 3D echocardiography

2. Background

In Landmark based Geometric Morphometrics, configurations are represented by $k \times m$ matrices, where k is the number of landmarks and m the dimension of the ambient space. When configurations are centered, a strict representation is given by $(k-1) \times m$ matrices. The space of each centered configuration, the so-called *Centered Configuration Space* $\mathcal{CC}_m^k$ can be identified with the linear space of the $(k-1) \times m$ matrices. On each point $X \in \mathcal{CC}_m^k$, representing a configuration, the tangent space $\mathcal{T}_X\mathcal{CC}_m^k$ is defined. A vector $V \in \mathcal{T}_X\mathcal{CC}_m^k$ represents a small deformation of the configuration X and can be represented, in turn, by a $(k-1) \times m$ matrix.

If one wants to filter out every rigid motion then rotations are removed, thus obtaining the *size-and-shape space* $S\Sigma_m^k = \mathcal{CC}_m^k/SO(m)$ as a quotient space with respect to the rotation's group.

If one wants to filter out the scaling too, then each *form* is scaled to unit *size*, thus obtaining

the *shape space* Σ_m^k. This is the reason upon which the geometry of the shape space depends on the choice of a size measure. As will be clear in the following this choice is not obvious.

In order to describe and compare different deformations it is very important to be able to decompose each deformation by projecting it on different subspaces of $\mathcal{T}_X\mathcal{CC}_m^k$, each one characterizing some important features of the deformation.

The aim of the present paper is to propose some useful decompositions of the tangent space $\mathcal{T}_X\mathcal{CC}_m^k$ in order to unify old and new methods in a unique framework. We prefer to formulate our decompositions in the tangent space to the centered configuration space, rather than in the tangent space to the shape space, as classically done, because we are interested in describing the whole deformation. In fact, changes in size are important descriptors of the deformations. We recall that a decomposition of a vector space is given if one defines different complementary subspaces. Each vector of the original vector space can be expressed in a unique way as a linear combination of elements belonging to the defined subspaces. We note that, in general, two subspaces can be complementary without being orthogonal each other, with respect to the Euclidean metric. Moreover, once given a decomposition of a vector space, it is always possible to define new metrics relatively to which the given subspaces are orthogonal.

In order to describe the deformation it is important to introduce some important subsets of $\mathcal{T}_X(\mathcal{CC}_m^k)$.

The first is the set $\mathcal{V}_u$ of the uniform deformations of X:

$$\mathcal{V}_u = \{V \in \mathcal{T}_X(\mathcal{CC}_m^k) : V = XH^T\,,\, H \in \mathcal{C}_m^m\}\}, \tag{2.1}$$

It describes the overall deformation of the reference configuration. We use the term *uniform* instead of the most used *affine* because affine includes also translations that are filtered out here.

There are other two very important subspaces that are, in turn, subspaces of $\mathcal{V}_u$: the *spherical* (homothetic) deformations of X $\mathcal{V}_{sph} \subset \mathcal{V}_u$ and the *small rotations* of X $\mathcal{V}_{rot} \subset \mathcal{V}_u$:

$$\mathcal{V}_{sph} = \{V \in \mathcal{T}_X(\mathcal{CC}_m^k) : V = \lambda X\,,\, \lambda \in \mathbb{R}\} \tag{2.2}$$

$$\mathcal{V}_{rot} = \{V \in \mathcal{T}_X(\mathcal{CC}_m^k) : V = XW\,,\, W \in \mathcal{C}_m^m\},\ W + W^T = 0\}. \tag{2.3}$$

While each one of the above mentioned subspaces has a direct characterization, there are two important subspaces, namely the set $\mathcal{V}_{nu}$ of the non-uniform deformations of X, and the set $\mathcal{V}_{nsph}$ of the non-spherical deformations of X, that admit only indirect definitions, as orthogonal complements. In particular:

$$\mathcal{V}_{nu} = \{V \in \mathcal{T}_X(\mathcal{CC}_m^k) : g(U,V) = 0\ \forall U \in \mathcal{V}_u\} \tag{2.4}$$

$$\mathcal{V}_{nsph} = \{V \in \mathcal{T}_X(\mathcal{CC}_m^k) : g(U,V) = 0\ \forall U \in \mathcal{V}_{sph}\}. \tag{2.5}$$

In such a way the following decompositions holds:

$$\mathcal{T}_X(\mathcal{CC}_m^k) = \mathcal{V}_u \oplus^g \mathcal{V}_{nu} = \mathcal{V}_{sph} \oplus^g \mathcal{V}_{nsph} \tag{2.6}$$

where $\oplus^g$ is the orthogonal sum *with respect to the metric tensor g*. In fact the *orthogonality* is not a concept given a priori but it is defined by the metric tensor. We want to stress that g depends on the considered point X then the *orthogonality* depends on X.

By defining the *deviatoric* component as the *uniform non spherical* component:

$$\mathcal{V}_{dev} \quad = \quad \mathcal{V}_{nsph} \cap \mathcal{V}_u \tag{2.7}$$

we obtain, in turn, the following orthogonal decomposition, w.r.t. g, on each configuration X:

$$\mathcal{T}_X(\mathcal{CC}_m^k) \quad = \quad \underbrace{\mathcal{V}_{rot} \oplus^g \overbrace{\mathcal{V}_{sph} \oplus^g \mathcal{V}_{dev}}^{\mathcal{V}_{nrot}}}_{\mathcal{V}_u} \oplus^g \mathcal{V}_{nu} \tag{2.8}$$

It is easy to understand that the above decomposition can be interpreted as a splitting of the (small) deformation in a component that changes only *orientation*, *size*, *shape* (affine and non affine Fig.2).

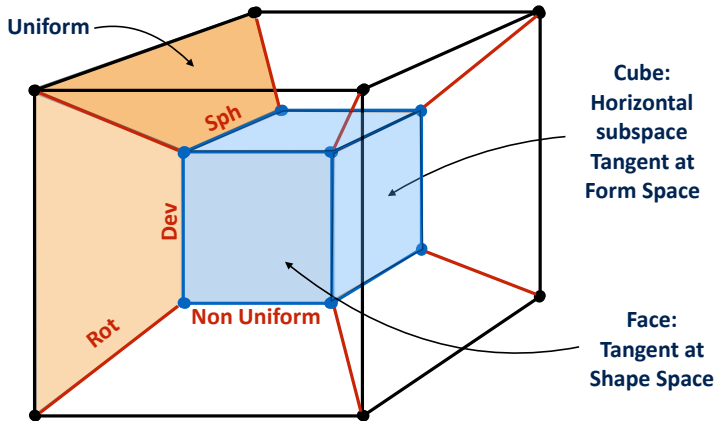

Figure 2: The fourfold decomposition of the tangent space defined in eq. 2.9 can be visualized through an 4-dimensional hypercube.

$$\mathcal{T}_X(\mathcal{CC}_m^k) \quad = \quad \underbrace{\mathcal{V}_{rot}}_{orientation} \quad \oplus^g \overbrace{\underbrace{\mathcal{V}_{sph}}_{size} \oplus^g \underbrace{\mathcal{V}_{dev} \oplus^g \mathcal{V}_{nu}}_{shape}}^{form} \tag{2.9}$$

.

Then, given a small deformation V_X of the configuration X, the rotational component V_{rot} must be filtered out by using a proper procedure of alignment (either Ordinary Procrustes Analysis (OPA) or Modified Ordinary Procrustes Analysis (MOPA) see below).

If one performs the quotient w.r.t. the rotation's group, for obtaining the *size-and-shape space* $S\Sigma_m^k = \mathcal{CC}_m^k / SO(m)$, the above decomposition can be interpreted as a decomposition in *vertical*

subspace ($\mathcal{V}_{rot}$) and *horizontal subspace* (the orthogonal complement $\mathcal{V}_{sph} \oplus^g \mathcal{V}_{dev} \oplus^g \mathcal{V}_{nu}$). The horizontal subspace on the configuration X represents (is isometric to) the tangent space to the size-and-shape space $S\Sigma_m^k$ at the *form* $[X]_S$, where $[X]_S$ is the equivalence class given by the action of $SO(m)$ on X.

Figure 1 shows the decomposition of the tangent space of the size-and-shape space $\mathcal{T}S\Sigma_m^k$. In particular the subspace named *non spherical tangent space* corresponds to the shape space tangent space $\mathcal{T}\Sigma_m^k$.

It is important to stress that the above decomposition, in general, relies on the choice of g. In particular, being $\mathcal{CC}_m^k$ globally a linear space, a possible choice of g could be the Euclidean dot product $g(U, V) = U \cdot V = \mathrm{Tr}(U^T V)$, as usually done in Procrustes analysis.

On the other hand, the choice of the Euclidean metric is not the sole possible.

While the definitions of rotation, scaling, and uniform deformation are independent from the choice of g, the definitions of *size*, *shape*, *non uniform deformation* depend on that choice.

In the next section we will discuss the definitions of *size* and *shape* by means of a very simple example: the size and shape space of the rectangles and we will show how that definitions are related to the choice of the metric tensor g.

3. Two universes for Size: size and shape of a rectangle

3.1. Coordinate systems and concepts of size and shape

What is the *size*? What is the *shape*? And how can we distinguish a *change in size* from a *change in shape*? In the present section we will discuss these issues by means of a very simple example: the family of rectangles centered in the origin and aligned with a cartesian coordinate system.

This family is characterized by symmetry with respect to both horizontal and vertical axes. It is simple to understand that each rectangle can be described by the coordinates of just one vertex, say (x_1, x_2), lying on the first quadrant $x_1 \geq 0, x_2 \geq 0$. In fact, once fixed the first landmark, the whole configuration matrix can be parametrized as:

$$X = \begin{pmatrix} x_1 & x_2 \\ -x_1 & x_2 \\ -x_1 & -x_2 \\ x_1 & -x_2 \end{pmatrix} \tag{3.1}$$

Then, we can say that the *size-and-shape space of rectangles* is a *two dimensional manifold* and the pair $(x_1, x_2) \in \mathbb{R}^+ \times \mathbb{R}^+$ is the trivial, cartesian, (upper right quadrant) coordinate system

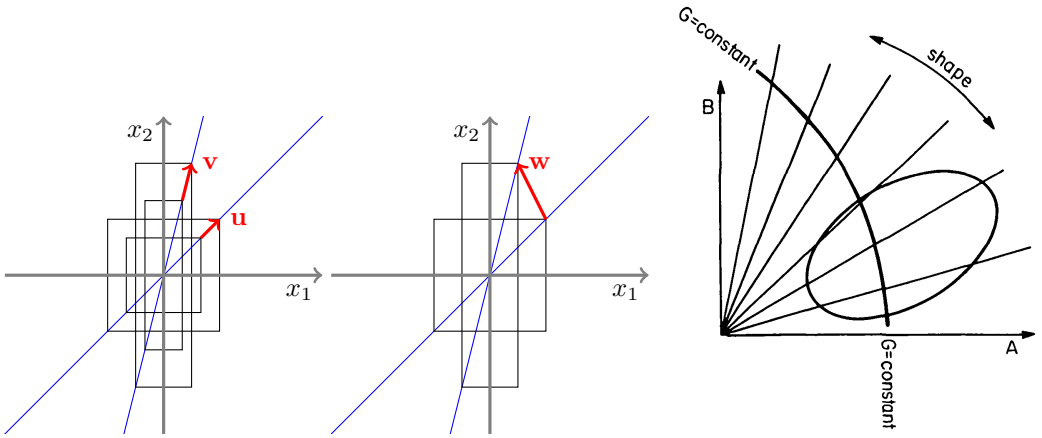

Figure 3: The left panel shows two different iso-shape vectors $\mathbf{u}, \mathbf{v}$ applied to different sources (a square and a rectangle) that are deformed into targets differing only for their (increased) size relatively to their proper source. Center panel show the iso-size vector $\mathbf{w}$ connecting two different shapes that have actually the same size (m-Volume in this case). Right panel reproduce original Bookstein' intuition about size and shape change (Bookstein, 1989b). "G" can represent any meaningful measure of size. Once defined it, the shape change becomes unambiguous under that size definition.

describing it (Figure 3 and 4). On the other hand this is not the unique possible coordinate system for the given space.

As we want to characterize two particular aspects (size and shape), we can ask if *it is possible to choose a different coordinate system in which one parameter represents the size and the second the shape*. In order to answer this, we can start by introducing two qualitative notions:

- A size measure $\sigma(X)$ is any positive real valued function of the configuration matrix such that $\sigma(aX) = a\sigma(X)$ for any positive scalar a.
- The shape must be associated to a quantity that *does not change* when we scale X to aX.

In this simple case it is trivial to say that the shape of a rectangle is quantified by the aspect ratio between height and width $\lambda = x_2/x_1$. In fact, when a rectangle enlarges without changing its shape, the first landmark moves along a straight line of slope λ (see Figure 3 left). Each straight line starting from the origin (Figure 3 and 4) is a *iso-shape* curve. Less obvious is to characterize the family of *iso-size* curves. In particular, each line cutting all the *iso-shape* curves could be a candidate to be an *iso-size* curve (see Figure 3 right).

On the other hand one could desire some additional requirements for choosing the *iso-size* curve. For example one could prefer an orthogonal coordinate system, because one wants to uncouple size and shape. This requirement brings to describe the *iso-size* curves as circumferences by relating the size directly to the Euclidean length of the segment joining the first landmark to the origin (see Figure 4 center). This is the most used definition of size in GM: the centroid size

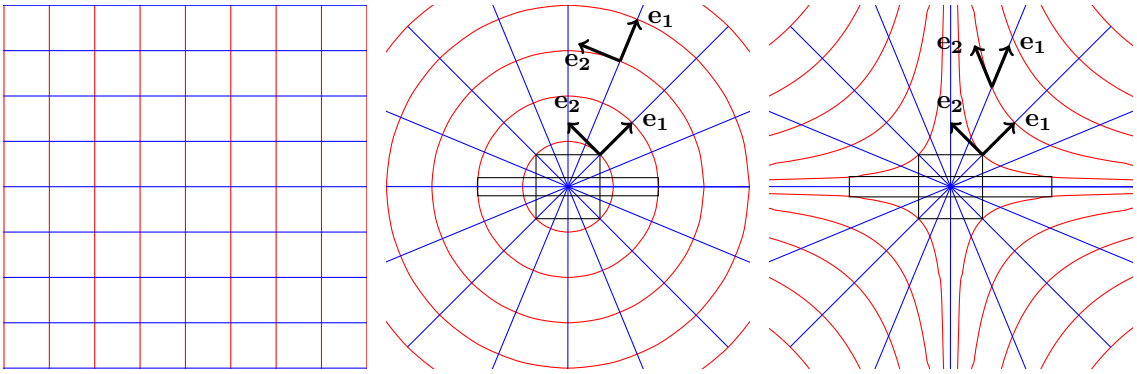

Figure 4: Different reference systems to illustrate change in shape while maintaining size according to different size definitions. Left panel illustrate a classic cartesian coordinate system. Center panel shows iso-size lines that maintains CS. Right panel shows a space where iso-size lines refer to the maintainance of m-Volume and are hyperbolic. The squares in the center and right panels are identical while the rectangles, that are deformations of the squares, are slightly different. The former has the same CS of the square, the latter the same m-Volume. The couples of vectors e1 and e2 show the directions of iso-size and iso-shape changes; they are identical, in center and right panels, in correspondence of the tangent to the square, while they visibly differ when evaluated in other positions. In particular, we note that in the case of CS maintainig reference system, being iso-size lines circular, e1 and e2 are always orthogonal (in Euclidean perspective), while it is not the case for the m-Volume maintaining space.

$CS = \sqrt{\mathrm{Tr}(X^T X)}$. In the particular case of rectangles, being X parametrized by (3.1), the size measure can be defined $\sigma_{CS}(X) = CS(X) = \sqrt{\mathrm{Tr}(X^T X)} = 2\sqrt{x_1^2 + x_2^2}$.

In GM is usual to fix the size at $\sigma_{CS} = 1$ in order to lie in the shape space. Figure 5 left shows as the shape space of rectangles can be represented by fixing the iso-size circumference of radius 1/2 (red line). The *distance* between two different rectangles should be measured walking on that circumference (blue line).

A different choice could be to define directly the size in terms of physical meaning. In this case the natural definition is that of m-Volume or, if one wants a quantity scaling linearly when X becomes aX, the mth-root of the m-Volume. In the rectangle' case the size is defined as $\sigma_{AR} = 2\sqrt{x_1\, x_2}$ and the *iso-size* curves are hyperbola (see Figure 4 right).

If we fix $\sigma_{AR} = 1$ we obtain a different shape space. Figure 5 right shows that in this case the shape space of rectangles can be represented by fixing the iso-size hyperbola defined by $x_1\, x_2 = 1/4$ (red line). The *distance* between two different rectangles should be measured walking on that hyperbola (blue line). This parametrization, although more physically meaningful suffers from three undesirables features:

- the *iso-size* curves are not convex
- the *iso-size* curves are not compact

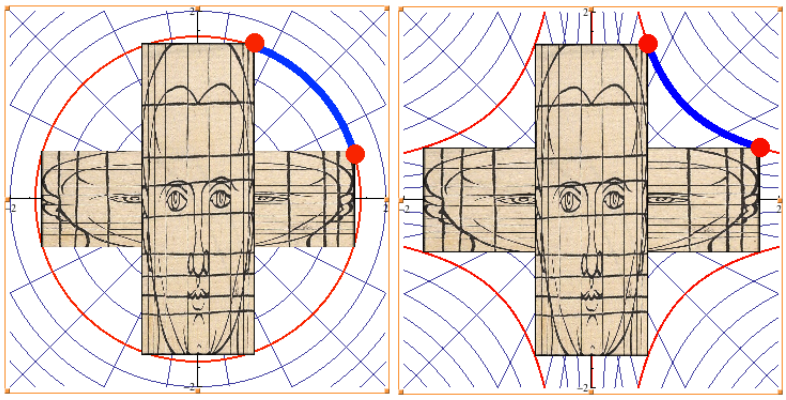

Figure 5: Distances (blue lines) between two configurations in the two subspaces that maintain, respectively, CS (left panel) or m-Volume (right panel).

- the *iso-size* curves are not orthogonal to the *iso-shape* curves

While the firsts two features could be annoying only for very slender rectangles (near to vertical or horizontal axes), the third feature seems to be the most problematic: the size and the shape changes are not uncoupled. But this problem can be easily circumvented by exploiting the fact that the orthogonality is not an intrinsic concept in a manifold (as the parallelism). The orthogonality is defined by the choice of a Riemannian metric on the manifold. In particular, the chosen parametrization is not orthogonal with respect to the Euclidean metric. In this context the Euclidean metric does not assume any physical meaning. It is very simple to build a metric with respect to which the given parametrization is orthogonal. This can be done in the following steps (see Table 1):

- build a field of basis $\mathbf{e}_1, \mathbf{e}_2$ tangent to the coordinate curves.
- build the field of the reciprocal basis $\mathbf{e}^1, \mathbf{e}^2$ so that $\mathbf{e}_\alpha \cdot \mathbf{e}^\beta = \delta_\alpha^\beta$, where $\alpha, \beta = 1, 2$.
- build the metric tensor as $g(\mathbf{u}, \mathbf{v}) = \mathbf{G}\mathbf{u} \cdot \mathbf{v}$, where $\mathbf{G} = \mathbf{e}^1 \otimes \mathbf{e}^1 + \mathbf{e}^2 \otimes \mathbf{e}^2$.

It is easy to verify that $g(\mathbf{e}_\alpha, \mathbf{e}_\beta) = \mathbf{G}\mathbf{e}_\alpha \cdot \mathbf{e}_\beta = \delta_{\alpha\beta}$, i.e. the system of coordinates is orthonormal with respect to the metric g.

Table 1 shows the outlined construction of the metric in the case of three different parametrizations (cartesian, centroid size, m-Volume). In the first two the resulting metric is the Euclidean one, while in the third case we obtain a non Euclidean metric tensor.

This procedure is satisfactory but can be proposed only for very simple cases as that of rectangles, in which is simple to define explicitly the bases.

Table 1: Three parametrizations

	Cartesian	Polar (Centroid Size)	Hyperbolic (m-Volume)
Parametrization	$\mathbf{x} = (x_1, x_2)$	$\mathbf{x} = \frac{\sigma_{CS}}{2}(\cos(\theta), \sin(\theta))$	$\mathbf{x} = \frac{\sigma_{AR}}{2}\left(\frac{1}{\sqrt{\tan(\theta)}}, \sqrt{\tan(\theta)}\right)$
Basis	$\mathbf{e}_1 = (1, 0)$ $\mathbf{e}_2 = (0, 1)$	$\mathbf{e}_1 = (\cos\theta, \sin\theta)$ $\mathbf{e}_2 = (-\sin\theta, \cos\theta)$	$\mathbf{e}_1 = (\cos\theta, \sin\theta)$ $\mathbf{e}_2 = (-\cos\theta, \sin\theta)$
Dual Basis	$\mathbf{e}^1 = \mathbf{e}_1$ $\mathbf{e}^2 = \mathbf{e}_2$	$\mathbf{e}^1 = \mathbf{e}_1$ $\mathbf{e}^2 = \mathbf{e}_2$	$\mathbf{e}^1 = \left(\frac{1}{2\cos\theta}, \frac{1}{2\sin\theta}\right)$ $\mathbf{e}^2 = \left(-\frac{1}{2\cos\theta}, \frac{1}{2\sin\theta}\right)$
Metric tensor	$\begin{pmatrix} 1 & 0 \\ 0 & 1 \end{pmatrix}$	$\begin{pmatrix} 1 & 0 \\ 0 & 1 \end{pmatrix}$	$\begin{pmatrix} \frac{1}{2\cos^2\theta} & 0 \\ 0 & \frac{1}{2\sin^2\theta} \end{pmatrix}$

where $\theta = \arctan x_2/x_1$, $\sigma_{CS} = 2\sqrt{x_1^2 + x_2^2}$, $\sigma_{AR} = \sqrt{x_1 x_2}$

3.2. A generalizable procedure (for affine component only)

One way to generalize the procedure sketched above toward more complicated cases is to observe that each deformation from a rectangle to a different one can be expressed as a linear transformation and, then, represented by a 2×2 matrix. In particular, it is possible to transform a rectangle of coordinates $\mathbf{x} = (x_1, x_2)$ into a deformed one of coordinates $\mathbf{x}+\mathbf{v} = (x_1, x_2)+(v_1, v_2) = (x_1 + v_1, x_2 + v_2)$ through the matrix:

$$\mathbf{A}_\mathbf{v} = \begin{pmatrix} \frac{x_1+v_1}{x_1} & 0 \\ 0 & \frac{x_2+v_2}{x_2} \end{pmatrix} = \begin{pmatrix} 1 + \frac{v_1}{x_1} & 0 \\ 0 & 1 + \frac{v_2}{x_2} \end{pmatrix} \tag{3.2}$$

If one subtracts the identity, it can be obtained the transformation associated to the displacement vector $\mathbf{v}$:

$$\mathbf{H}_\mathbf{v} = \mathbf{A}_\mathbf{v} - \mathbf{I} = \begin{pmatrix} \frac{v_1}{x_1} & 0 \\ 0 & \frac{v_2}{x_2} \end{pmatrix} \tag{3.3}$$

This can be done for each $\mathbf{v} \in \mathbb{R}^2$ by defining, in this way, an isomorphism between $\mathbb{R}^2$ and the tangent space to the lie group of the diagonal matrices 2×2.

Using this correspondence one can obtain, starting from the basis $\mathbf{e}_\alpha$, a basis in the space of of the diagonal matrices 2×2:

$$\mathbf{H}_{\mathbf{e}_1} = \frac{1}{\sigma_{CS}} \begin{pmatrix} 1 & 0 \\ 0 & 1 \end{pmatrix} \qquad \mathbf{H}_{\mathbf{e}_2} = \frac{1}{\sigma_{CS}} \begin{pmatrix} -1 & 0 \\ 0 & 1 \end{pmatrix} \tag{3.4}$$

Then $\mathbf{H}_{\mathbf{e}_1}$ is a spherical matrix, while $\mathbf{H}_{\mathbf{e}_2}$ is a deviatoric (traceless) one. This two matrices are orthogonal with respect to the dot product between matrices. This means that, by using this

representation, the change in shape is naturally uncoupled by the change in m-Volume. In fact, it is well known that deviatoric matrices represent small deformations that do not change m-Volume. Then, by means of the built isomorphism one can inherit the dot product from the matrices by obtaining a Riemannian metric in $\mathcal{V}$ as follows:

$$g(\mathbf{v},\mathbf{u}) = \mathbf{H_v}\cdot\mathbf{H_u} = \mathrm{Tr}(\mathbf{H_v}^T\mathbf{H_u}) = \frac{u_1v_1}{x_1^2} + \frac{u_2v_2}{x_2^2} \tag{3.5}$$

It is easy to verify that $g(\mathbf{e}_\alpha,\mathbf{e}_\beta) = \delta_{\alpha\beta}\frac{2}{\sigma_{CS}^2}$, thus we obtained an orthogonal parametrization. If we prefer an *orthonormal* parametrization, we can define the metric as:

$$g(\mathbf{v},\mathbf{u}) = \frac{\sigma_{CS}^2}{2}\mathbf{H_v}\cdot\mathbf{H_u} \tag{3.6}$$

As we will show in the following, this procedure is generalizable to k landmarks in m dimensions.

We note that the procedure explained above can be applied only to affine transformations. The issues related to the non affine component will be faced in the next section.

4. A general conceptualization of size and shape change

With reference to Figure 1 we are interested to characterize two decompositions:

Uniform vs Non Uniform

Spherical vs Non Spherical

Given a configuration X, and a deformation vector $V \in \mathcal{T}_X(\mathcal{CC}_m^k)$ we may define an infinitesimally deformed configuration Y by:

$$Y = X + V\,. \tag{4.1}$$

The deformation vector V can be decomposed in an overall uniform part and a non uniform one:

$$V = V_u + V_{nu} \tag{4.2}$$

If we assume Y aligned with X, $V_{rot} = 0$ and V can be decomposed in a spherical component and a non spherical one:

$$V = V_{sph} + V_{nsph}$$

As explained in section 2, using both decompositions one obtains:

$$V = V_{sph} + V_{dev} + V_{nu}$$

$$V = \underbrace{V_{sph} + V_{dev}}_{V_u} + V_{nu} = V_{sph} + \underbrace{V_{dev} + V_{nu}}_{V_{nsph}} \tag{4.3}$$

In order to obtain the three components, starting from V, we need to characterize three orthogonal projectors to choose a metric g. In section 3, with reference to the rectangle's case, we discussed two different choices for g. The Euclidean choice was suitable to describe change in size as change in Centroid Size, where the non Euclidean choice was suitable to describe change in size as change in m-Volume. In the *platonic* case of rectangles a very simple explicit formulation was possible because the reference configuration was trivial and only uniform deformations were allowed.

In particular, in the case of rectangles, it is easy to calculate both the *increments* in size (CS or m–Volume) and the *actual values* of the size (CS or m–Volume).

In order to expand both approaches to the general case, it is important to note that:

- In general 3D cases the calculation of the *actual value* of the CS is always possible using the definition CS=$\sqrt{\mathrm{Tr}(X^T X)}$. Different CS values correspond to different iso-size hyper surfaces, that, in particular, are hyper spheres in the $m(k-1)$ linear space. The hypersphere of unit radius (once removed rotations), is the shape space.

- On the other hand, calculating the *actual value* of the m-Volume in 3D is not possible by means of simple algebraic manipulations of the matrix X.

- The calculation of the *increment* in m-Volume given by a deformation V is instead possible in two steps:

  1) calculation of the uniform component $V_u = VH^T$ of V

  2) calculation of the trace of the matrix H associated to the uniform component of V

Then the definition of a metric coherent with the size increment as m-Volume increment needs a preliminary definition of the decomposition in uniform and non uniform components.

4.1. Unifying strategies for decomposition of deformations in one formalism

In the present section we characterize the decomposition of the deformation vector V, according to 4.2 in an overall uniform part and a non uniform one. This decomposition can be performed in different ways (Bookstein, 1989; Rohlf, F.J. and Bookstein, F.L. , 2003). A general representation could be:

$$\begin{aligned} V_u &= XH^T \\ V_{nu} &= \Phi W \end{aligned} \tag{4.4}$$

where $H = A - I$ is the $m \times m$ matrix representing the uniform transformation, Φ is a $(k-1)\times(k-1)$ symmetric matrix which can represent an interpolating function and W is a $(k-1)\times m$ matrix parametrizing the non uniform component. The matrices H and W can be obtained as $H^T = \Gamma_{21} V$

and $W = \Gamma_{11} V$, with

$$\begin{aligned} \Gamma_{21} &= \left(X^T \Phi^{-1} X\right)^{-1} X^T \Phi^{-1} \\ \Gamma_{11} &= \Phi^{-1} - \Phi^{-1} X \Gamma_{21} \end{aligned} \tag{4.5}$$

see (Bookstein, 1989; Dryden, I.L., Mardia, K.V., 1998, 2016). The choice of Φ implies different representations. In the following we consider only two cases:

- $\Phi = I$. This corresponds to define the uniform component through the pseudo inverse (the *regression method* of (Rohlf, F.J. and Bookstein, F.L. , 2003), sections 10.2 and 12.5 of (Dryden, I.L., Mardia, K.V., 1998) .
- $\Phi = S$, as defined in eqn. (1). This corresponds to define the uniform component through the thin plate spline representation ((Bookstein, 1989), (Dryden, I.L., Mardia, K.V., 1998), section 10.3).

We note that in the second case the matrix Γ_{11} is the so called *bending energy matrix*.

The two different definitions are not equivalent from many points of view.

- the first choice (pseudo inverse) leads to a decomposition that is orthogonal with respect to the Euclidean metric, the second does not.
- the first choice does not allow the use of deformation grids as it is a function not defined in the whole ambient space, the second allows them.
- the first choice is not based on an energetic criterion as the second one.

see Table 2 for attributes of the two approaches.

Table 2: Two decompositions

	Compatible with Euclidean metric	Interpolation based	Energy based
Pseudoinverse	YES	NOT	NOT
TPS	NOT	YES	YES

By using (4.4), (4.2) can be rewritten as:

$$V = X\Gamma_{21} V + \Phi \Gamma_{11} V \tag{4.6}$$

where $X\Gamma_{21}$ and $\Phi\Gamma_{11}$ are two complementary projectors (see proof in Appendix 1).

4.2. Unifying Procrustes metric and bending energy metric in one formalism

As we showed in the example of rectangles, a decomposition of the tangent space can be built by deciding some important features, independently from the fact that the resulting subspaces

are orthogonal or not with respect to the Euclidean metric. In a second step one can build a Riemannian metric coherent with the given decomposition, i.e. such that the decomposition results to be orthogonal with respect to the new metric.

As sketched in section 3.2, in the case of uniform transformations, a metric compatible with the definition of size as m-Volume should be the metric induced by the inner product between the $m \times m$ matrices of uniform transformations. The generalization of this concept consists in defining the metric evaluated on two deformations U, V as the dot product between the two matrices H_U and H_V of their uniform components. This is a pseudo metric because defined only on the subspace of uniform deformations:

$$g_u(U,V) := g_u(U_u, V_u) = \mu_1 \left(H_U \cdot H_V\right) = \mu_1 \mathrm{Tr}\left(H_U^T H_V\right) = \mu_1 \mathrm{Tr}\left(U^T \Gamma_{21}^T \Gamma_{21} V\right) \tag{4.7}$$

where $\mu_1 \in \mathbb{R}^+$ is a positive coefficient. In order to obtain a nonsingular metric we need also a metric defined only on the nonuniform component. First of all we observe that the Euclidean product between the non uniform components of U, V gives:

$$U_{nu} \cdot V_{nu} = \Phi\Gamma_{11} U \cdot \Phi\Gamma_{11} V = \mathrm{Tr}\left(U^T \Gamma_{11} \Phi^2 \Gamma_{11} V\right) \tag{4.8}$$

When $\Phi = I$ the above expression becomes simply $V_{nu} \cdot U_{nu} = \mathrm{Tr}\left(V^T \Gamma_{11} U\right)$. Then we propose the following expression for the non uniform component metric:

$$g_{nu}(U,V) := g_{nu}(U_{nu}, V_{nu}) = \mu_2 \mathrm{Tr}\left(V^T \Gamma_{11} U\right) \tag{4.9}$$

where $\mu_2 \in \mathbb{R}^+$ is a positive coefficient. When $\Phi = I$, this expression corresponds to the Euclidean product between the non uniform components of U, V, while for $\Phi = S$ it gives the inner product between U, V weighted by the bending energy matrix.

Finally, we propose a general representation for the complete metric tensor, suitable for different situations:

$$g(U,V) := \mathrm{Tr}\left(U^T G^\alpha V\right) \tag{4.10}$$

where

$$G := \mu_1 \Gamma_{21}^T \Gamma_{21} + \mu_2 \Gamma_{11} = G_u + G_{nu} \tag{4.11}$$

$\mu_1, \mu_2 \in \mathbb{R}^+$ can be functions of the undeformed configuration X, and the exponent $\alpha \in (0,1)$ can be set for giving the Euclidean ($\alpha = 0$) or non Euclidean ($\alpha = 1$) metrics. In fact for $\alpha = 0$ $G^\alpha = I$, whatever the values of μ_1 and μ_2. These parameters characterize the vector lengths in the affine and non affine subspaces, respectively, in the case of $\alpha = 1$.

Table 3 summarizes the different strategies that can be adopted when combining the various Φ and α.

Table 3: Three Methods

	$\alpha = 0$	$\alpha = 1$
$\Phi = I$	Fully Euclidean	Generalized Pseudoinverse procedure (GPp)
$\Phi = S$	NOT ALLOWED	Thin Plate Spline space (TPSs)

Once defined the metric g, we can project the deformation vector along the direction of the homothety (represented by the *unit vector* $X/\sqrt{g(X,X)}$) and on the orthogonal complement, thus obtaining:

$$V_u = V_{sph} + V_{dev} \tag{4.12}$$

where

$$\begin{aligned} V_{sph} &= g\left(V, \frac{X}{\sqrt{g(X,X)}}\right)\frac{X}{\sqrt{g(X,X)}} = \frac{g(V,X)}{g(X,X)}X \\ V_{dev} &= V_u - V_{sph} \end{aligned} \tag{4.13}$$

It is worth noting that in the case called "Fully Euclidean", the magnitude of V_{sph} represents the increment of CS, while in both GPp and TPSs it represents the increment of m-Volume.

4.3. Unifying rotations definitions in one formalism: OPA and MOPA

A general technique of alignment between two forms $[X]_S$ and $[Y]_S$ is based on the minimization of the distance defined as:

$$d([X]_S,[Y]_S) = \inf_{Q\in SO_m} \sqrt{g\left((YQ-X),(YQ-X)\right)} = \inf_{Q\in SO_m} \sqrt{\mathrm{Tr}\left((YQ-X)^T G^\alpha (YQ-X)\right)}\,.$$

Where g can be chosen as explained above. The *aligned configuration* $\hat{Y}$ is obtained by means of an *optimal rotation* $\hat{Q}$ minimizing d.

$$\hat{Y} = Y\hat{Q}$$

where $\hat{Q} = \text{argmin}\ \ g\left((YQ-X),(YQ-X)\right)$. According to this definition, $\hat{Q}$ turns out to be the rotational component of the polar decomposition of Y^TGX.

When $\alpha = 0$ we obtain the rotational component of Y^TX (the classical Ordinary Procrustes Analysis (OPA) (Dryden, I.L., Mardia, K.V., 2016)). When $\alpha = 1$ then $Y^TGX = H$, i.e. the rotational component of the uniform part of the deformation, calculated through the pseudo inverse or the TPS. In the latter case we define the alignment Modified OPA (MOPA) (Varano et al., 2017).

4.4. Evaluation of the percentages

Define the percentages

$$sph_{\%} = \frac{g(V_{sph},V_{sph})}{g(V,V)}, \quad dev_{\%} = \frac{g(V_{dev},V_{dev})}{g(V,V)} \quad nu_{\%} = \frac{g(V_{nu},V_{nu})}{g(V,V)}$$

where $g(V,V) = g(V_{sph}, V_{sph}) + g(V_{dev}, V_{dev}) + g(V_{nu}, V_{nu})$

4.5. Meaning and estimation of the coefficients μ_1 and μ_2

Looking at the structure of the metric tensor G (4.11), it is clear that μ_1 and μ_2 must depend only on the undeformed configuration X, being the metric tensor a characteristic of the tangent space in X. Moreover, while the orthogonality between the three components (spherical, deviatoric, non uniform), is encoded in the structure of the projectors $\Gamma_{21}^T\Gamma_{21}$ and Γ_{11}, the values of the coefficients μ_1 and μ_2 characterizes the weight, in the total length of the deformation vector, assigned to the uniform and non uniform components, respectively.

While in the Fully Euclidean case the values of the coefficients μ_1 and μ_2 are immaterial, in the non Euclidean one they must be calibrated coherently with the choice of the interpolating function Φ.

4.5.1. Generalized Pseudoinverse procedure (GPp)

In the GPp $\Phi = I$ i.e. the uniform component is evaluated through the pseudo inverse, as in the Fully Euclidean approach, then the uniform and non uniform subspaces are orthogonal also with respect to the Euclidean metric. As previously seen, by setting $\mu_2 = 1$ in this case the metric of the non uniform subspace is Euclidean too. The unique difference between GPp and Fully Euclidean is in the structure of the uniform metric. This is built by using the dot product in the space of the linear transformations in such a way that the deviatoric component is related to transformations that don't change the m-Volume (instead of CS). This structure determines only the direction of the spherical or deviatoric components. The lengths are determined by μ_1. As the non uniform metric is Euclidean, in order to make the lengths in the uniform subspace comparable with that in the non-uniform one, we calibrate μ_1 by imposing that the length of a spherical deformation be equal to their Euclidean length, i.e.:

$$g_u(\lambda X, \lambda X) = \mu_1 \lambda^2 \mathrm{Tr}\left(H_X^T H_X\right) = \mu_1 \lambda^2 \mathrm{Tr}\left(I\right) = \mu_1 \lambda^2 m \tag{4.14}$$

$$\lambda X \cdot \lambda X = \lambda^2 \mathrm{Tr}\left(X^T X\right) = \lambda^2 CS^2 \tag{4.15}$$

then

$$g_u(\lambda X, \lambda X) = \lambda X \cdot \lambda X \rightarrow \mu_1 = \frac{CS^2}{m} \tag{4.16}$$

Finally, for GPp we set: $\mu_1 = \frac{CS^2}{m}$ and $\mu_2 = 1$

4.5.2. Thin Plate Spline space (TPSs)

In the TPSs $\Phi = S$, i.e. the decomposition in uniform and non uniform components is performed by means of the Thin Plate Spline. The TPS method is an interpolation method based on the minimization of the so called *bending energy* J, gauging the second derivative of the displacements. In particular, given a body, represented in the undeformed configuration, by the regular

region Ω of $\mathbb{R}^m$, we label $\mathbf{x}$ the points in Ω and $\mathbf{y}$ the points in the deformed configuration Ω_t at the instant t. If the configurations are sampled in k landmarks, then Ω can be represented by the $k \times m$ matrix X and Ω_t by the deformed configuration Y. The displacement field is represented by the difference vectors:

$$\mathbf{u} = \mathbf{y} - \mathbf{x} \tag{4.17}$$

In the landmark case the displacements experienced by the k landmarks can be collected in the $k \times m$ matrix $U = Y - X$.

The bending energy is defined as: $J = \int_{\mathbb{R}^m} \nabla\nabla\mathbf{u} \cdot \nabla\nabla\mathbf{u}$.

The bending energy can be considered as a pseudo-distance because it gauges the difference between two configurations but it is singular on the affine deformations. Moreover it is non symmetric in the sense that $J(X, Y) \neq J(Y, X)$. A nonsingular distance, inspired by the continuum mechanics, and used in the deformable templates method (Younes, 2010), is the strain energy φ.

We define the *strain* energy

$$\varphi = \frac{1}{2} \int_{\Omega} \mathbf{E} \cdot \mathbf{E} \tag{4.18}$$

where

$$\mathbf{E} = \frac{\nabla\mathbf{u} + \nabla\mathbf{u}^T}{2} \tag{4.19}$$

The strain energy lives naturally in a continuum context, while the bending energy lives in a landmark based context but does not gauge uniform deformations. Moreover the strain energy is defined as an integral on the body domain, while the bending energy is defined as an integral on the whole $\mathbb{R}^m$, which does not diverges because the curvature of the TPS grid, outside of Ω, decays quickly to zero. In order to compare the two energies here we introduce the *body-bending energy*, defined as $J_\Omega = \int_\Omega \nabla\nabla\mathbf{u} \cdot \nabla\nabla\mathbf{u}$. In general the bending energy will be slightly greater than the body-bending energy and we introduce the *decay* $\rho = J/J_\Omega$.

There exists a relationship between strain energy and body-bending energy? It is easy to show that, while for a general deformation they assume different values, there exist at least one example in which the two energies are identical. The simplest case of non uniform deformation is that in which a rectangle bends in a trapezoid: a bilinear transformation. That can be realized by assigning a bilinear displacement:

$$\mathbf{u} = [(\chi \otimes \mathbf{B})\,\mathbf{x}]\mathbf{x} \tag{4.20}$$

where $\mathbf{B} = \mathbf{e}_1 \otimes \mathbf{e}_2$ and $\chi = \chi_1\mathbf{e}_1 + \chi_2\mathbf{e}_2$ are the bending with respect to the two axes.

$$\nabla\mathbf{u} = [\chi \otimes (\mathbf{B} + \mathbf{B}^T)]\mathbf{x} \qquad\qquad \nabla\nabla\mathbf{u} = \chi \otimes (\mathbf{B} + \mathbf{B}^T) \tag{4.21}$$

In this particular case $\nabla\nabla\mathbf{u}$ is constant and than holds:

$$\nabla\mathbf{u} = [\nabla\nabla\mathbf{u}]\,\mathbf{x} \tag{4.22}$$

and the strain energy can be calculated easily as:

$$\varphi = \frac{1}{2}\int_\Omega \nabla\mathbf{u}\cdot\nabla\mathbf{u} = \frac{1}{2}\int_\Omega \left([\nabla\nabla\mathbf{u}]\,\mathbf{x}\cdot[\nabla\nabla\mathbf{u}]\,\mathbf{x}\right) \tag{4.23}$$

$$= \frac{1}{2}[(\chi\cdot\chi)\int_\Omega \mathbf{x}\cdot\mathbf{x}\,dA] = \frac{1}{2}(\chi_1^2+\chi_2^2)\mathcal{I}_p \tag{4.24}$$

where $\mathcal{I}_p$ is the polar inertia of Ω calculated with respect to the centroid. on the other hand the body-bending energy is:

$$J_\Omega = \int_\Omega \nabla\nabla\mathbf{u}\cdot\nabla\nabla\mathbf{u} = 2(\chi\cdot\chi)\mathcal{A} = 2(\chi_1^2+\chi_2^2)\mathcal{A} \tag{4.25}$$

where $\mathcal{A}$ is the area of Ω. We can note that, in this case:

$$\varphi = \frac{\mathcal{I}_p}{4\mathcal{A}}J_\Omega = \frac{\mathcal{I}_p}{4\rho\mathcal{A}}J \tag{4.26}$$

According to (Varano et al., 2017) in 2D problems

$$J = 16\pi\mathrm{Tr}\left(U^T\Gamma_{11}U\right) \tag{4.27}$$

we obtain

$$\varphi = \frac{4\pi\mathcal{I}_p}{\rho\mathcal{A}}\mathrm{Tr}\left(U^T\Gamma_{11}U\right) \tag{4.28}$$

The strain energy is directly proportional to the bending energy and the proportionality coefficient depends only on geometrical quantities of Ω together with the decay coefficient of the TPS. Because in this case the expression of the TPS gives an analytic solution it is possible to find the explicit expression of the decay:

$$\rho = \frac{2\pi\beta}{(1+\beta^2)\log(1+\beta^2)-\beta^2\log(\beta^2)} \tag{4.29}$$

where $\beta = L/H$.

In the case of 2D bilinear transformations the strain energy can be evaluated by means of the bending energy matrix, using a suitable coefficient depending on the geometry of Ω.

What happen with uniform deformations? In this case:

$$\mathbf{y} = \mathbf{A}\mathbf{x} \tag{4.30}$$

and the gradient of the displacement is constant:

$$\nabla\mathbf{u} = (\mathbf{A}-\mathbf{I}) = \mathbf{H} = \Gamma_{21}U \tag{4.31}$$

When U is mopa-aligned with the source H is symmetric then $E = H$. it follows

$$\varphi(U) = \frac{1}{2}\int_\Omega \mathbf{H}\cdot\mathbf{H} = \frac{1}{2}m - Volume(\Omega)\mathbf{H}\cdot\mathbf{H} = \frac{\text{m-Volume}(\Omega)}{2}\mathrm{Tr}\left(U^T\Gamma_{21}^T\Gamma_{21}U\right) \tag{4.32}$$

In the case of uniform transformations the strain energy can be evaluated by means of the symmetric matrix $\Gamma_{21}^T\Gamma_{21}$, using a suitable coefficient depending on the geometry of Ω.

The above consideration, concerning linear and bilinear transformations of rectangles, leads to define a new energy, able to reconcile the strain energy with the bending energy:

the Γ-energy, defined as the complete metric g introduced in the previous sections evaluated on the pair (U, U):

$$\Gamma(U) = g(U,U) = g_u(U,U) + g_{nu}(U,U) = \mu_1 \mathrm{Tr}\left(U^T\Gamma_{21}^T\Gamma_{21}U\right) + \mu_2 \mathrm{Tr}\left(U^T\Gamma_{11}U\right) \tag{4.33}$$

The first term $\mu_1 \mathrm{Tr}\left(U^T\Gamma_{21}^T\Gamma_{21}U\right)$ is called here *stretching energy* while the second term $\mu_2 \mathrm{Tr}\left(U^T\Gamma_{11}U\right) = \mu_2\frac{J}{\nu\pi}$ where $\nu = 16$ for $m = 2$ and is $\nu = 8$ for $m = 3$ (Varano et al., 2017) is then proportional to the *bending* energy J.

In the case of a general deformation of a rectangle described by only 4 landmarks in a trapezoid, the Γ-energy coincides with the strain energy if one set:

$$\begin{aligned} \mu_1 &= \frac{\mathcal{A}}{2} \\ \mu_2 &= \frac{16\pi\mathcal{I}_p}{4\rho\mathcal{A}} = \frac{4\pi\mathcal{I}_p}{\rho\mathcal{A}} \end{aligned} \tag{4.34}$$

$$\rho = \frac{2\pi\beta}{(1+\beta^2)\log(1+\beta^2) - \beta^2\log(\beta^2)} \tag{4.35}$$

where $\beta = L/H$.

It is important to stress that, for more general deformations, the Γ-energy does not coincides with the strain energy. It is only a concept that allows to sum, with a meaningful ratio, the stretching energy with the bending energy, in such away that one can evaluate suitable values for μ_1 and μ_2 for comparing the magnitude of a uniform deformation with the magnitude of a non uniform deformation.

We could consider the Γ-energy $\Gamma(U)$ as the strain energy $\varphi(\tilde{U})$ evaluated on a more simple deformation $\tilde{U}$ characterized by the same uniform component $\tilde{U}_u = U_u$ of U and a bilinear deformation $\tilde{U}_{nu}$ storing the same bending energy of U_{nu}, i.e. such that $J(\tilde{U}_{nu}) = J(U_{nu})$.

In order to obtain this equivalence one should set $\mu_1 =$ m-Volume/2, while the calculation of μ_2 is slightly more complicated.

When the decomposition of deformation is performed on a couple of shapes only, the value of μ_2 can be estimated by calculating numerically the strain energy and than imposing the equivalence between the gamma energy and the strain energy $\Gamma(U) = \varphi(U)$.

$$\Gamma(U) = g_u(U,U) + g_{nu}(U,U) = g_u(U,U) + \mu_2\frac{J}{\nu\pi} = \varphi(U) \rightarrow \mu_2 = \frac{\varphi(U) - g_u(U,U)}{\frac{J}{\nu\pi}} \tag{4.36}$$

If one deals with a *series* of deformations of the same source, the value of μ_2 must be estimated using an optimization approach aimed at finding the optimal value common to all decompositions

in order to make them comparable: for each decomposition between the same source and the i^{th} target the strain energy, stretching energy and bending energy are computed; then all values are used in the regression model ((strain energies-stretching energies)$\sim$bending energies/$(\nu\pi)$). The β coefficient of this model can be used as optimal μ_2 value common to the entire deformation series that starts from the same source.

In order to illustrate this, we anticipate here the μ_2 optimization procedure of the deformation of a regular parallelepiped reported below. The regular parallelepiped is deformed in 30 deformed states and each deformation is decomposed. Using formula 4.36 the strain energy and gamma energy are collinear but not equal (Fig. 6 left). Using the β coefficient of regression model estimated in Fig. 6 (center) as μ_2, we found a very satisfactory relationship between strain energy and gamma energy (Fig. 6 right).

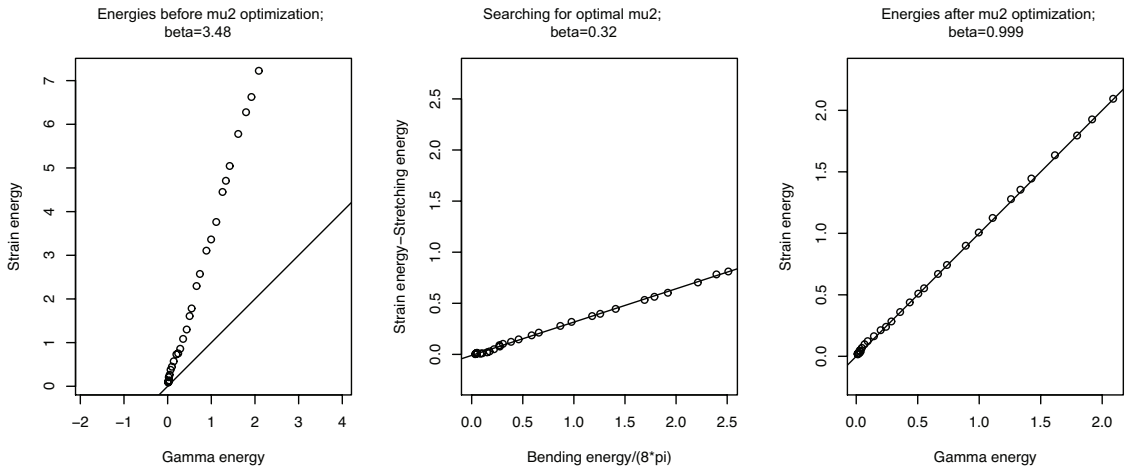

Figure 6: The procedure used in order o find a common μ_2 when dealing with a deformation series estimated from the same source. In this case we show results relative to the 3D experiment (see below). The same rationale applies to the 2D case. We calculated bending energy, stretching energy, strain energy and gamma energy for any deformation in the series using the initial value of μ_1= m-Voume/2 and μ_2=polar inertia/m-Volume. We can see that strain energy and gamma energy are collinear but not equal (left panel). By regressing (strain energy-stretching energy) on bending energy/(8π) we found the beta coefficient (0.32 in this case) to use as a common μ_2 value in the procedure of decomposition of deformation for each source *vs.* each ith deformed state. After that we found strain energy and gamma energy virtually identical. Continuous black line indicates isometry.

5. Theoretical simulations

We will provide here below a series of controlled explicit simulations aimed at showing the different decomposition strategies explained above. Both affine and non affine transformations are treated individually. Finally, we will show simulations where the spherical component is mixed with affine or non affine transformations. For each simulation we perform decompositions using both Euclidean and non Euclidean strategy (GPp and TPSs) following the classification illustrated

by Table 3. Moreover, we decomposed the deformations starting from the first configuration of the transformation series and using a sequential comparison. While the former approach bears a larger error during the projection on the tangent space (to the first configuration), the latter mitigates this error when moving along the deformation sequence.

This allows appreciating the curvature attributes as identified by different Riemannian metrics.

5.1. Aspect ratio change preserving m-Volume or CS in rectangles

The first simulation concerns two families of rectangles characterized, respectively, by the constraints:

- Centroid Size preserving: $\sqrt{B^2 + H^2} = 2$
- m-Volume preserving: $BH = 2$

where B is the base length and H is the height. Rectangles are generated by deforming a square identified by 4 landmarks and maintaining the CS or the m-Volume by modifying B/H ratio (Fig. 7). The initial square has side=$\sqrt{2}$, m-Volume=2 and CS=2. Deformations follow a series of thirty equally spaced values in the series $\theta \in [0.1, \pi/2 - 0.1]$, by using the polar and hyperbolic parameterizations shown in Table 1, respectively. We must remember here that μ_1 and μ_2 values come, in these particular cases, from the explicit formulas 4.34 as the shapes involved are all deformations of a general rectangle for which explicit μ_1 and μ_2 values can be computed. Results relative to the affine size-preserving experiment where components of deformation are computed from the square are shown in Fig. 8. It appears evident that when the decomposition starts from the square the three methods returns identical results within the categories of CS constant or m-Volume constant. This happens because the subspaces associated to the vector's decomposition are identical when estimated in correspondence of the square' landmarks as shown in Fig. 4. At that points the tangent to the circumference and that to the hyperbola are identical as shown in Fig. 4 (center and right panels). The non affine part is always zero as expected being the simulation built only upon uniform transformations. The small differences between CS constant and m-Volume constant are evident at the initial and final positions of the deformation series, where CS constant shows a smaller spherical component and a larger deviatoric component. This is due to the fact that in the two cases the extreme rectangles are not the same in the CS preserving and m-Volume preserving series as evident from Fig. 9 (left and center left panels). They actually have the same aspect ratio but being forced to maintain CS or m-Volume within their proper series they have inevitably different sizes in terms of CS or m-Volume when compared one with each other. Toward their central positions the CS preserving and m-Volume preserving series behave similarly and there the spherical part is close to 0 as expected in a size-preserving experiment.

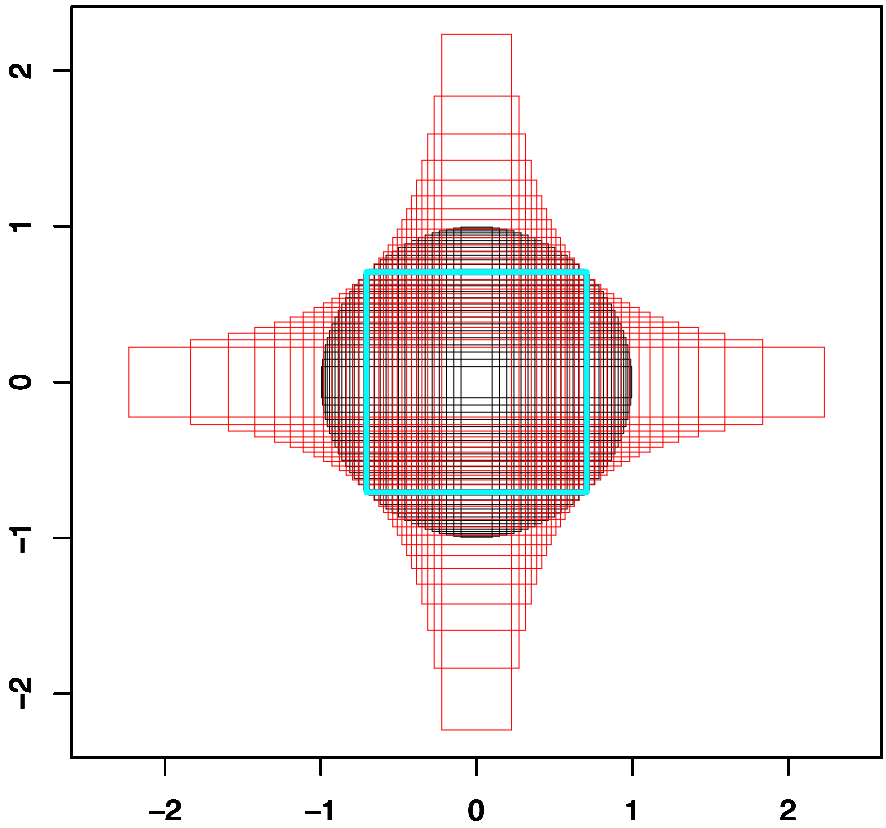

Figure 7: Rectangles generated by the deformations of the cyan square identified by 4 landmarks used in the CS or m-Volume maintenance affine simulations. The cyan square has side=$\sqrt{2}$, m-Volume=2 and Centroid Size=2. Aspect ratio is parameterized in order to maintain m-Volume (red shapes) or CS (black shapes).

Results relative to the affine size-preserving experiment where components of deformation are computed from the initial individual of each series are shown in Fig. 10. Here the sources from which components of deformation are computed are different in CS preserving or m-Volume preserving series. As first it must be noted that the Fully Euclidean approach applied to m-Volume constant series returns an incoherent result: in fact, the spherical component appears to be the dominant one, an unexpected result in a size-preserving transformation. This can be explained by looking at Fig. 9 (right panel): there the source (cyan) configuration (=the first rectangle of the series) is deformed in the 24^{th} rectangle of the series. We used the "Fully Euclidean" approch to decompose the deformation vector. This means using a circumferential space tangent to the source. According to this subspace the decomposition finds the spherical vector, i.e. that orthogonal to the circumeference, much larger than that tangent to it, i.e. the deviatoric one. In practice, in Fig. 9 right panel, we tried to adapt a metric built on a circumferential subspace to a deformation series built by moving along an hyperbola as shown in Fig. 4 (right panel). The opposite happens for CS preserving series decomposed according to GPp or TPSs approaches.

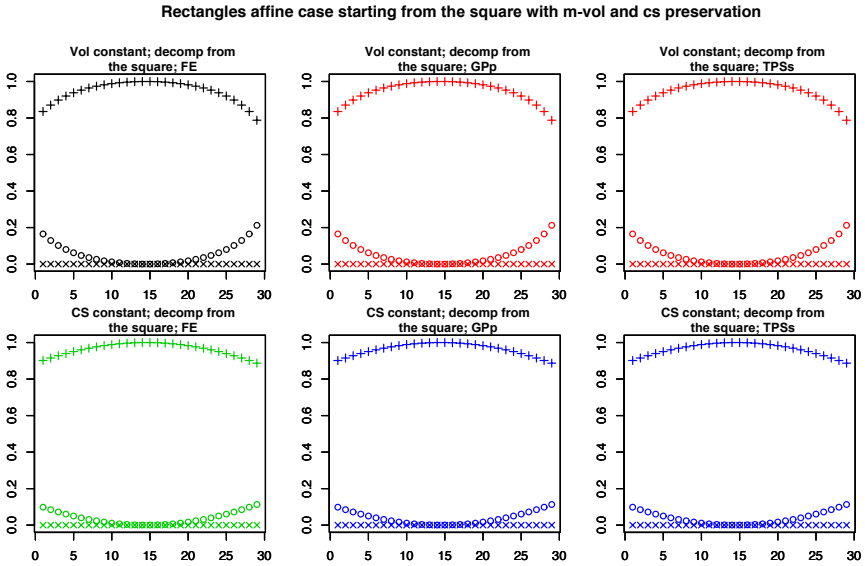

Figure 8: Results of decomposition of deformation using the regular square as fixed source by applying the Fully Euclidean approach, GPp and TPSs for the two deformation series, e.g. CS maintenance and m-Volume maintenance. As the tangent to the square is equal for both CS maintaining space and m-Volume maintaining space (as shown in Fig. 3) all these results are almost identical. See text for further details; "o" symbol indicates the spherical component; "x" symbol indicates the non affine component; "+" symbol indicates the deviatoric component.

There the deformation occurring in a series built by moving along a circumferential space is decomposed using the hyperbola tangent to the source, see Fig. 9 center-right panel. In this case the source (cyan=the first rectangle of the CS preserving series) is deformed on the 2^{th} rectangle of the series and the decomposition using the hyperbola returns approximately equal spherical and deviatoric components as quantified in Fig. 10 (bottom center and bottom right panel).

Fig. 11 shows the results relative di decompositions made in sequential fashion. In this case the manifolds (hyperbola or circumference) are approximated by the tangent spaces that depend on the approach used. When the decomposition approach is coherent with the subspaces used for building the deformation series the spherical and non affine components are always =0, while the deviatoric one is always =1. In the other cases this does not happen: when the Fully Euclidean approach is applied to the m-Volume constant series the curves start from the same values obtained when decomposing from the first series element. Toward the center of the series the components have the expected contributions(about 0% for spherical and non affine components and about 100% for the deviatoric one). This happens because towards the series center we find the quasi-square shapes and the decomposition performs similarly if done using hyperbola-based (=GPp and TPSs) or circumference-based (Fully Euclidean) metrics.

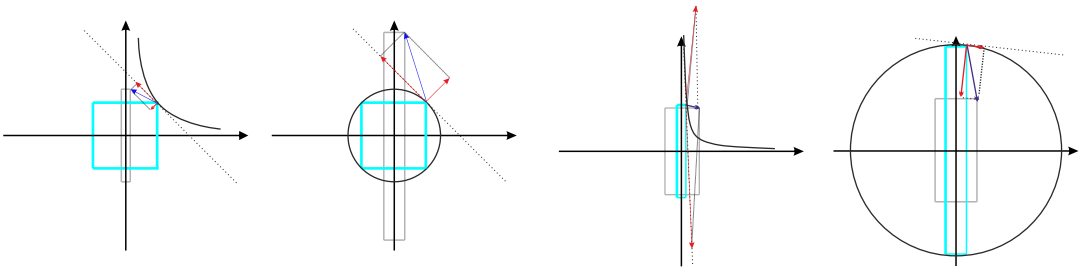

Figure 9: Decomposition of deformation vectors in iso-size and iso-shape components when the "inappropriate" reference system is applied to data generated following the preservation of size defined under a different iso-size reference system. Left panel shows the decomposition starting from the square with one of the most (affine) deformed states of the CS preserving series, e.g. the 24th shape, by using the tangent to hyperbolic iso-size line instead to the circumferential one under which data were generated. The blue vector is the total deformation vector and it is decomposed into orthogonal components (in red) along the tangent built on the hyperbola. The same is done in the center left panel where the decomposition between the rectangle and the 24th deformed state of preserving m-Volume series is illustrated using the tangent to the circumferential iso-size line instead of the hyperbolic one under which the data were generated. The two tangents are the same but the deformations and, consequently its components, are slightly different from the left panel due to the fact that the targets are different. The center right panel shows the decomposition from the first shape of CS preserving series toward the 2th deformed shape. Again, the tangent is built on the inappropriate (hyperbolic) iso-size line. The same is done for m-Volume preserving data in the right panel.

5.2. General Trapezoid

Each centered trapezoid can be generated starting from a centered rectangle (here constituted by 24 landmarks), by using the following formula:

$$\mathbf{y} = \mathbf{x} + \mathbf{H}\mathbf{x} + [(\chi \otimes \mathbf{B})\,\mathbf{x}]\mathbf{x} \tag{5.1}$$

where $\mathbf{H}$ is a 2×2 matrix, $\mathbf{B} = \mathbf{e}_1 \otimes \mathbf{e}_2$ and $\chi = \chi_1\mathbf{e}_1 + \chi_2\mathbf{e}_2$ are the bending with respect to the two axes.

Our dataset has been generated by means of (5.1), by randomly choosing thirty values among uniform distributions: $H_{11} \in [-0.1, 0.6], H_{12} \in [-0.1, 0.6], H_{21} \in [-0.1, 0.6], H_{22} \in [0, 0.3], \chi_1 \in [0, 0.3], \chi_2 \in [0, 0.3]$. Fig.12 shows the resulting shapes together with their proper m-Volume and CS values.

Figs. 13, 14 and 15 show results relative to the decomposition from the regular rectangle and its deformed states illustrated in Fig.12. The three methods perform differently. As for percentages shown in Fig. 13, the Fully Euclidean approach always shows the percentages of spherical component larger than Gpp or TPSs. On the other hand, both GPp and TPSs present the non affine component larger than the Fully Euclidean approach. However, the two methods differ for the emphatization of the deviatoric component that is larger in GPp approach. As for the maintainance of spherical component we plotted the ratio between the m-Volume (or CS) of

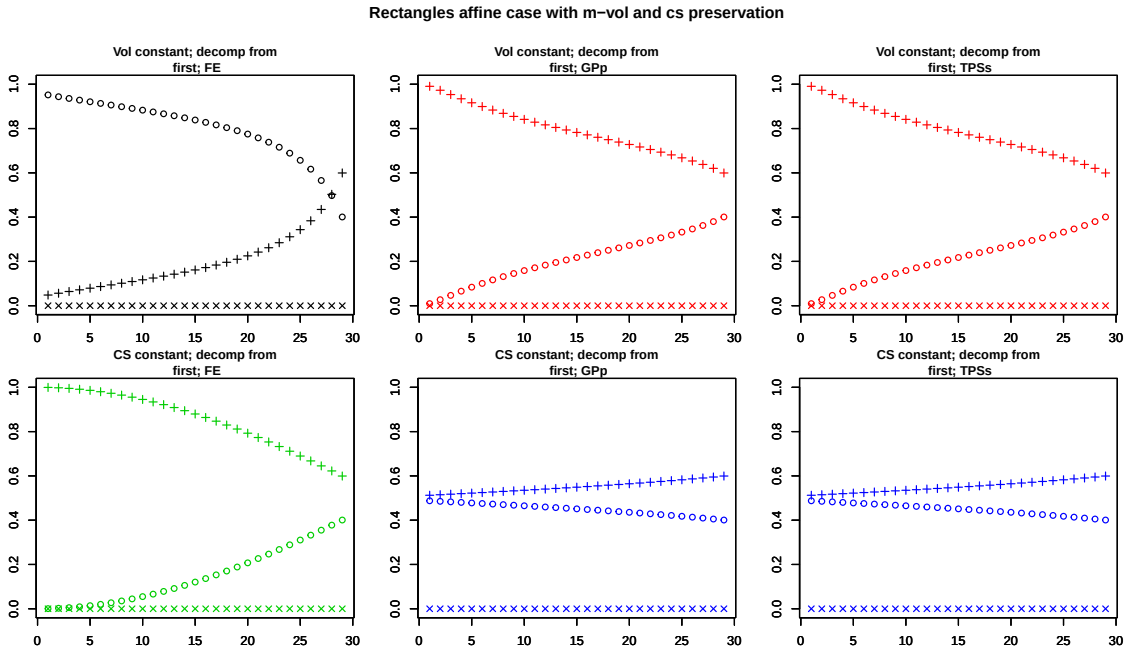

Figure 10: Results relative to the affine size-preserving experiment where components of deformation are computed from the initial individual of each series. Here the sources are fixed within CS preserving or m-Volume preserving series but these two sources are different between each other; "o" symbol indicates the spherical component; "x" symbol indicates the non affine component; "+" symbol indicates the deviatoric component.

original source and the i^{th} shape of the deformation series against the ratio between the m-Volume (or CS) of original source and the i^{th} configuration associated to spherical, deviatoric or non affine component. This configuration was obtained by summing to the source (i.e. the rectangle) the i^{th} component (spherical, deviatoric or non affine) of deformation series. The m-Volume, instead is maintained in the neighbour of 1, while it is overestimated for deviatoric configurations associated to deformations whose areas are larger than that of source (i.e. at abscissa's values smaller than 1). On the opposite, the non affine configurations always maintain a nearly constant ratio value of 1 (Fig.14). In particular, we can see that in the neighbour of 1 GPp and TPSs perform better than the Fully Euclidean approach that does not return expected values. It is evident that CS ratio is maintained close to 1 for deviatoric and non affine configurations as expected (Fig.15).

5.3. General three dimensional bilinear deformations.

In three dimensions bi-linear transformations can represent bending and torsion around three axes. A general representation is:

$$\mathbf{y} = \mathbf{x} + \mathbf{u} = \mathbf{x} + \mathbf{H}\mathbf{x} + (\mathbb{H}\mathbf{x})\mathbf{x} \tag{5.2}$$

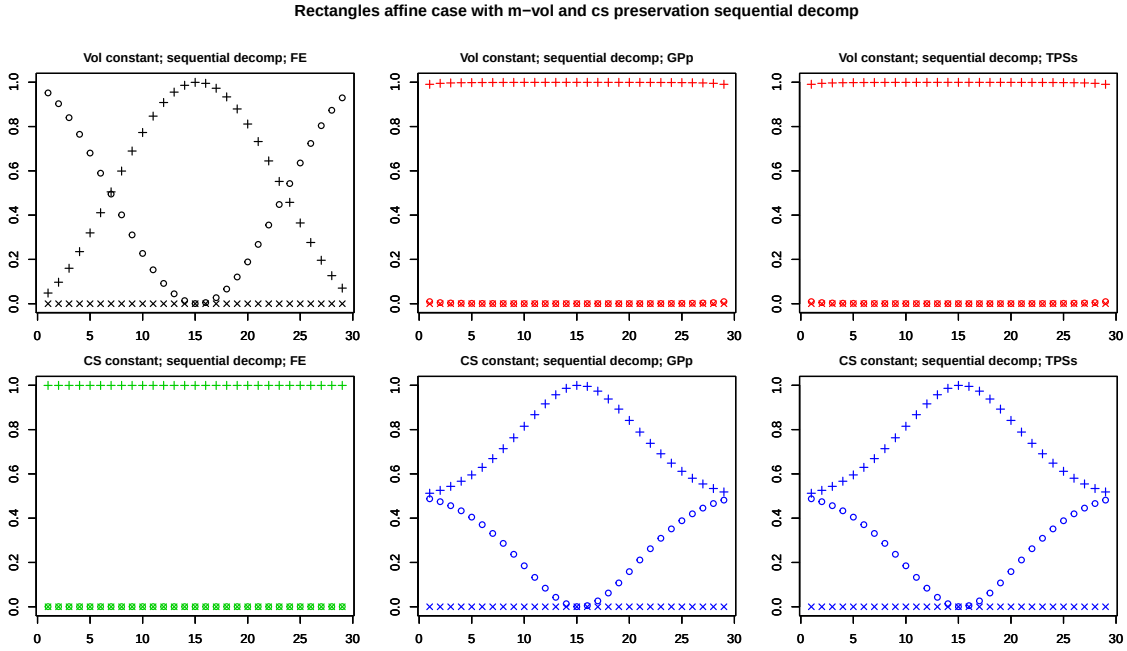

Figure 11: Results relative to decompositions made in sequential fashion. In this case the three approach returns different results in CS or m-Volume preserving data; "o" symbol indicates the spherical component; "x" symbol indicates the non affine component; "+" symbol indicates the deviatoric component.

where $\mathbf{H}$ is a 3×3 matrix and

$$\mathbb{H} = (\mathbf{W}_i(\mathbf{I} - \mathbf{e}_i \otimes \mathbf{e}_i)) \otimes \mathbf{e}_i \tag{5.3}$$

$$\mathbf{W}_i = \begin{pmatrix} 0 & -\chi_{3i} & \chi_{2i} \\ \chi_{3i} & 0 & -\chi_{1i} \\ -\chi_{2i} & \chi_{1i} & 0 \end{pmatrix} \tag{5.4}$$

where χ_{ii} is the amount of the torsion around the i-axis, and χ_{ij} is the bending in the plane $\mathbf{e}_i, \mathbf{e}_j$.

Our dataset has been generated by means of (5.3), starting from a parallelepiped ($L = B = 1, H = 5$) defined by 30 landmarks as shown in Fig.16, by randomly choosing thirty values among uniform distributions: $H_{11} \in [-0.04, 0.24], H_{12} \in [-0.04, 0.24], H_{21} \in [-0.04, 0.24], H_{22} \in [-0.04, 0.24], \chi_{11} \in [-0.04, 0.24], \chi_{12} \in [-0.04, 0.24], \chi_{13} \in [-0.04, 0.24], \chi_{21} \in [-0.04, 0.24], \chi_{22} \in [-0.04, 0.24], \chi_{23} \in [-0.04, 0.24], \chi_{31} \in [-0.04, 0.24], \chi_{32} \in [-0.04, 0.24], \chi_{33} \in -0.04, 0.24]$. Fig.16 shows the resulting shapes together with their proper m-Volume and CS values.

Figs 17, 18 and 19 shows results relative to the decompositions from the regular parallelepiped to its deformed states illustrated in Fig.16. The three methods perform differently. The Fully Euclidean approach ("centroid size based" and thus "non energy based") intensifies the contribu-

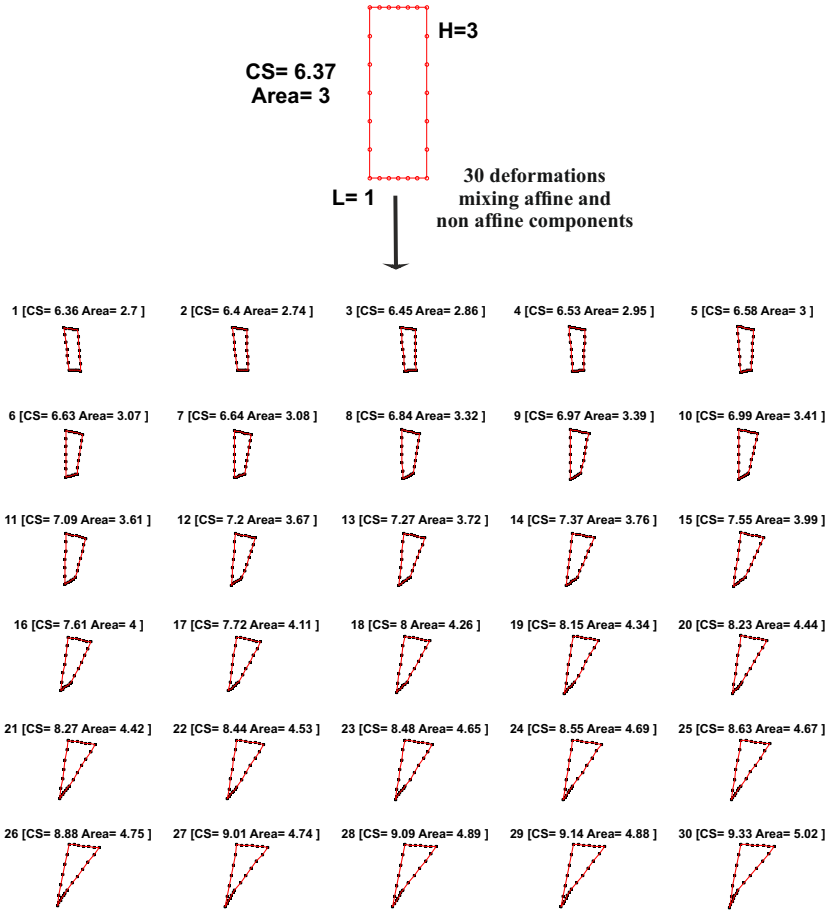

Figure 12: 2D data used for simulation where both affine and non affine deformations are mixed together. The regular rectangle is deformed into 30 states. m-Volume and CS of each configuration are indicated.

tion of the spherical component, while the non affine and the deviatoric ones are less important. GPp ("m-Volume based" and still "non energy based") and TPSs ("m-Volume based" and "energy based") methods furnish a different view: the spherical component is the less important for both methods, while they differ in the way they weight the affine and non affine components. In particular, TPSs emphasizes the non affine one whereas GPp emphasizes the affine part. This can be explained upon the fact that TPSs use an energetic criterion to give differential weights to affine and non affine components. As the non affine transformations are concentrated locally, they are better evaluated using bending energy and for this reason they receive more weight in TPSs than in GPp (or even in Fully Euclidean approach) that uses the Euclidean length to weight components. The behaviour of m-Volume and CS maintainance is consistent for what seen in the 2D example.

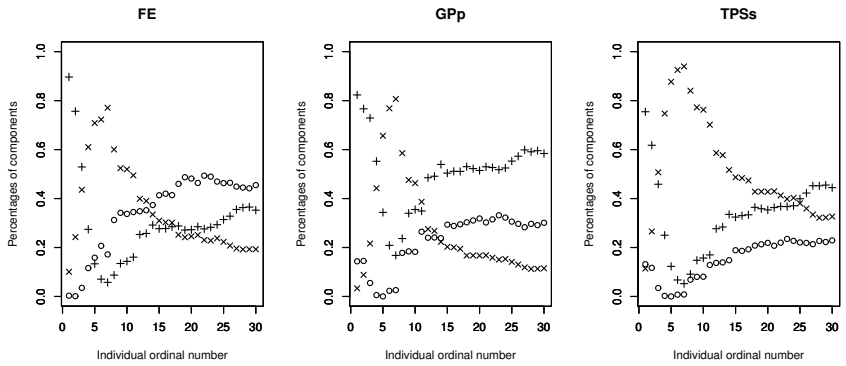

Figure 13: Percentages of components, under the three methods, for 2D data with mixed affine and non affine deformations. In this case all decompositions are performed using the regular rectangle as fixed source; "o" symbol indicates the spherical component; "x" symbol indicates the non affine component; "+" symbol indicates the deviatoric component.

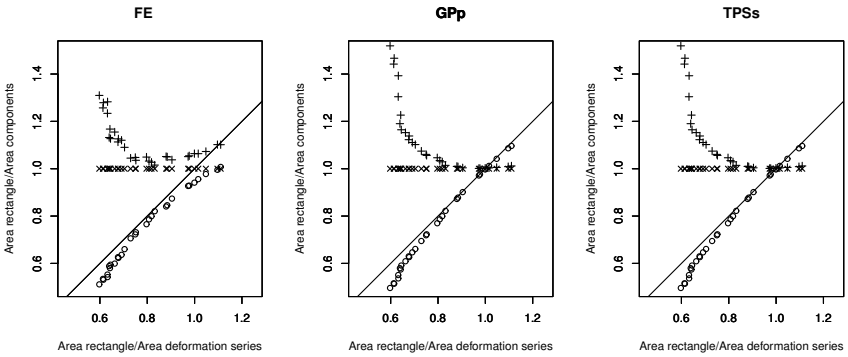

Figure 14: Ratio betwen the m-Volume of the source (regular rectangle) and that of the shape associated to any individual component (spherical, deviatoric or non affine) plotted vs. the ratio between source' m-Volume and that of its actual deformed state"o" symbol indicates the spherical component; "x" symbol indicates the non affine component; "+" symbol indicates the deviatoric component.

6. Medical example: Left Ventricle Mechanics

In order to show a real model intimately related to the problems illustrated above, we present here a cardiological example that illuminates the importance of deformation' decomposition in the context of Left Ventricle (LV) shape analysis and mechanics. We use here (in a different manner) the same data used in (Madeo et al., 2015) to identify trajectories attributes in Hypertrophic Cardiomyopathy (HCM). We contrasted the deformations occurring in epicardium and endocardium in the Control subjects sample (n=46) and in HCM patients (n=20). We performed the decomposition on the entire LV trajectory thus on shapes evaluated at 16 electromechanically homologous times defined in (Piras et al., 2017). In Supplementary Information S1 we illustrated and explained the homologous time's interpolation. This allows to compare different phases of several individuals

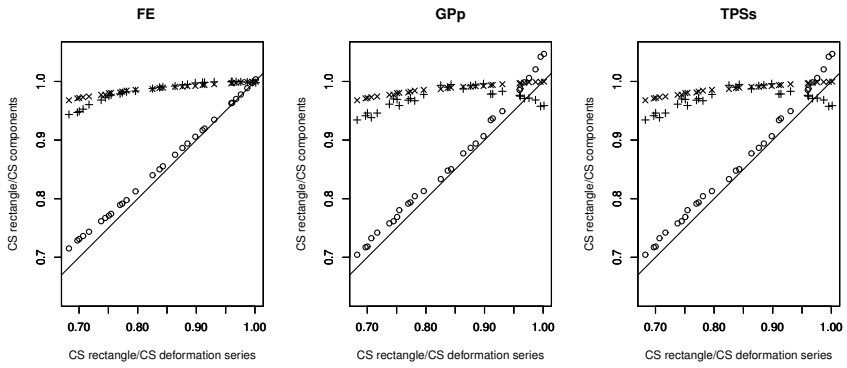

Figure 15: Ratio betwen the CS of the source (regular rectangle) and that of the shape associated to any individual component (spherical, deviatoric or non affine) plotted vs. the ratio between source' CS and that of its actual deformed state; "o" symbol indicates the spherical component; "x" symbol indicates the non affine component; "+" symbol indicates the deviatoric component.

at physiologically homologous time frames. We contrasted the ability in recognizing pathology for the Fully Euclidean and TPSs methods. We did this in order to ease the readability of results and because the GPp method is intermediate between the above mentioned approaches. For each method (Fully Euclidean and TPSs) and for each homologous time we performed a classification exercise using a permutated version of the common machine learning technique "Support Vector Machine" (SVM) that randomizes data splitting. The 46 Controls and 20 HCM cases were randomly split into a training dataset of 12 Control and 12 HCM used for learning and a test dataset of 34 Control and 8 HCM used for classification. This splitting was nearly unavoidable in order to have a balanced design during the learning phase. This was done 1000 times in order to produce a large amount of classifications performed on completely unknown data. At each run, the 32 Control and 8 HCM randomly chosen test cases were classified using the function estimated upon the corresponding training dataset. Using the resulting specificity and sensitivity we calculated the Area Under the Curve (AUC) of the Receiver Operating Characteristic (ROC) curve. The mean AUC values over all runs were retained as representative of global classification performance. We performed the same bulk of analyses using epicardium/endocardium as dependent binary variable. In this case, given that the response variable had different sample sizes for Control and HCM (i.e. 46 epi and 46 endo for Control and 20 epi and 20 endo for HCM) we used for learning 22 epi and 22 endo for Control and 12 epi and 12 endo for HCM. This particular analysis has no a clinical meaning but a physiological/mechanical one as it is aimed at unveiling deformational differences between the two LV layers. In fact, a very important question was introduced in (Evangelista et al., 2015) related to epicardial and endocardial composing LV wall: in a previous investigation using the finite element model of a human LV (Evangelista et al., 2011) they studied how to measure the so called *Principal Strain Lines* (PSLs) (Gabriele et al., 2014, 2015). It was found

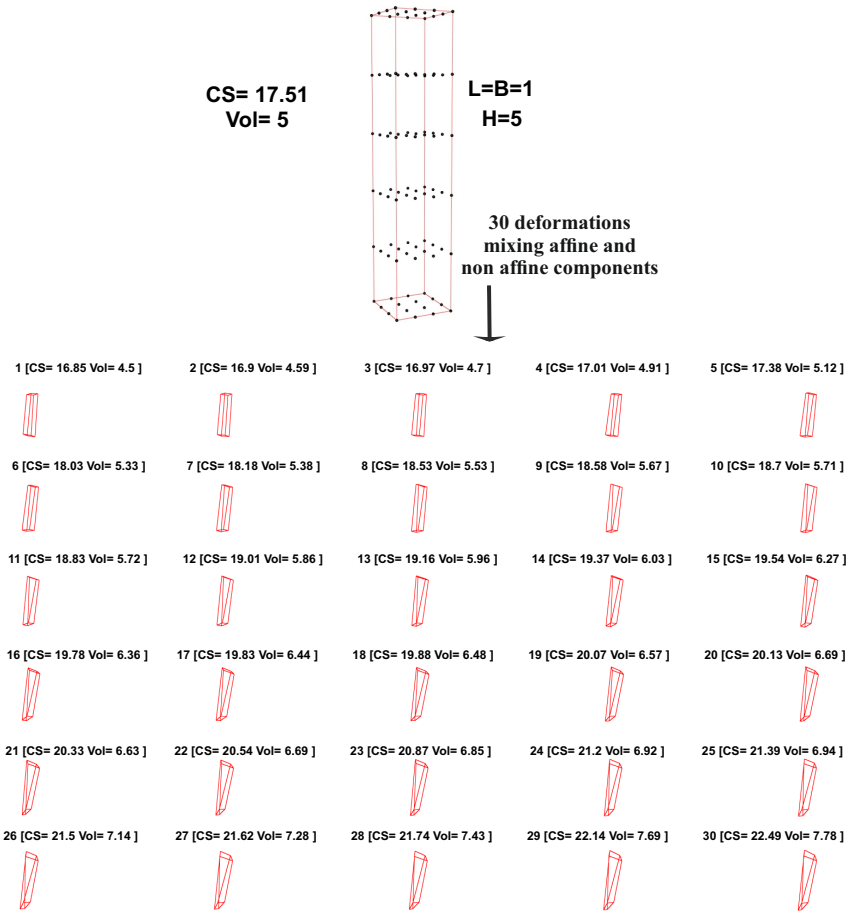

Figure 16: 3D data used for simulation where both affine and non affine deformations are mixed together. The regular parallelepiped is deformed into 30 states. m-Volume and CS of each configuration are indicated.

that endocardial PSLs are circumferential, so identifying functional strain lines whose direction is different from the hypothesized direction of the muscle fibers which in the model spiral clockwise, sharing an angle with the circumferential direction.

On the contrary, it was found that epicardial PSLs agree with muscle fiber directions, which in the model spiral counterclockwise toward the base. The mechanical interpretation of these results is based on the idea that the driving forces of the LV deformative process are muscle contraction and blood pressure, and the contraction-driven component of the deformation process sets serious compatibility issues (given by surfaces curvature), affecting mainly subendocardium layers due to their higher geometrical stiffness ((Nardinocchi et al., 2012)). In order to explain this concept it may be useful to imagine the myocardium as divided into two semi-independent layers (endocardium and epicardium), each one moving independently with respect to the other and having uniformly oriented fiber. In this situation, muscle contraction would induce a large counter-clockwise (clockwise) rotation of the epicardial (endocardial) layer ((Nardinocchi et al.,

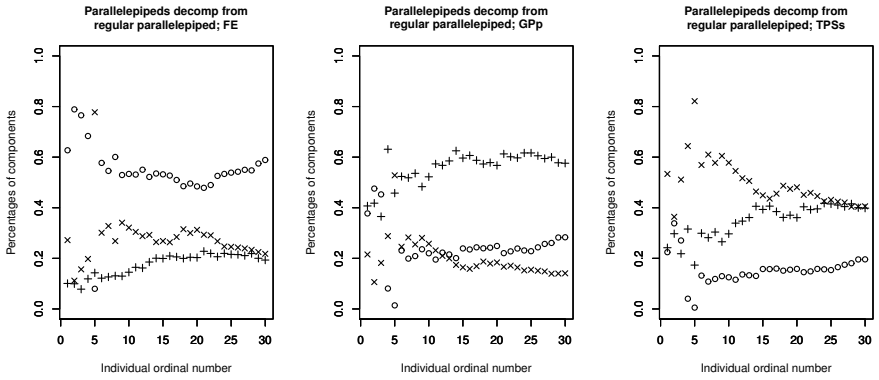

Figure 17: Percentages of components, under the three methods, for 3D data with mixed affine and non affine deformations. In this case all decompositions are performed using the regular parallelepiped as fixed source; "o" symbol indicates the spherical component; "x" symbol indicates the non affine component; "+" symbol indicates the deviatoric component.

2012)), and we simply would find that PSLs, on each layer, are determined by fiber directions. Actually, the two layers cannot move independently, due to compatibility (ensuring the continuity of the material), and muscle orientation changes smoothly from the subepicardium to the subendocardium; moreover, the larger radius of rotation for the outer epicardial layer assigns to epicardial fibers a mechanical advantage in dominating the overall direction of rotation (Sengupta et al., 2009). Hence, only epicardial deformations are rotation-driven whereas endocardial and subendocardial layers, having a smaller rotation (due to the smaller radius of rotation or, it is the same, to the larger geometrical stiffness), deform mainly along the circumferential and the longitudinal direction, with the circumferential shortening larger than the longitudinal one due to LV geometry. In terms of decomposition of deformation it implies that, relatively to the total deformation, the percentage of affine component is larger than that of the non affine one for the endocardium while it holds the opposite for the epicardium mainly affected by non affine deformation (i.e. torsion among other transformations). Thus, the endocardium experiences more spherical (=homothetic) and deviatoric (=aspect ratio or shear) components in relation to its proper total deformation. On the other hand, the epicardium deforms mainly according to the well known torsional (i.e. non affine) dynamics described in the most of echocardiographical studies. We test these hypotheses by quantifying components of deformation in Control and HCM LVs.

Important differences emerge when looking at Fig. 20 where, along the entire cycle, we plotted the AUC relative to Control/HCM and endocardium/epicardium identification for percentages of individual components (spherical, deviatoric and non affine) for Fully Euclidean and TPSs methods. While here only AUCs are plotted, Supplementary Information S1 shows the complete distributions of data (with significances and effect sizes under ANOVAs) associated to each homologous time. A more synthetic picture is given by Fig. 21 where AUC values refer to the classification

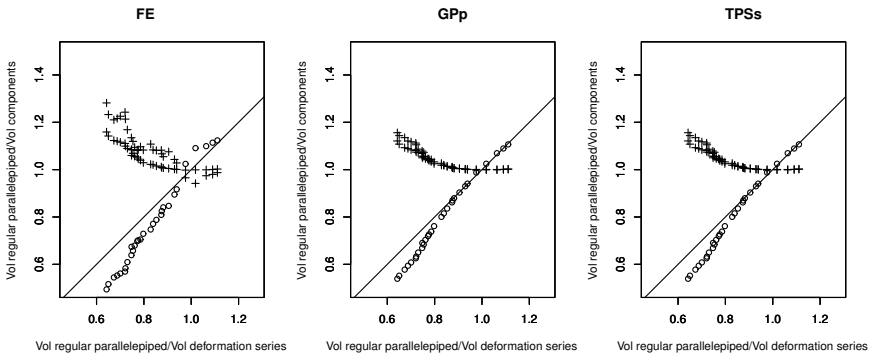

Figure 18: Ratio betwen the m-Volume of the source (regular parallelepiped) and that of the shape associated to any individual component (spherical, deviatoric or non affine) plotted vs. the ratio between source' m-Volume and that of its actual deformed state; "o" symbol indicates the spherical component; "x" symbol indicates the non affine component; "+" symbol indicates the deviatoric component.

power of the three components combined together. Given that our homologous times have the diastole in first position and systole in fifth position, the systo-diastolic decomposition is that corresponding to the fourth position. It emerges that both methods are effective in finding differences both for Control from HCM and for epicardium from endocardium. The two approaches are more efficient in discriminating epicardum from endocardium in comparison to pathology detection. In the former case the TPSs method seems better than the Fully Euclidean approach mainly during the mesodiastolic and telediastolic phases while in sistole they perform smilarly. On the opposite, the Fully Euclidean approach recognizes HCM pathology better than TPSs. This is particularly evident looking at 21 where the AUCs relative to the combinations of the three components are illustrated. These results offer the possibility to choose the method that better agrees with the initial null hypothesis and that reflects the mechanical or clinical aim of specific investigations. We suggest that the Fully Euclidean method is preferable for HCM' pathology detection while TPSs has a more mechanical meaning as it better separates, on average during the entire LV'cycle, epicardium from endocardium in both Control and HCM subjects. This can be appreciated in Fig. 22 where only epicardium/endocardium comparisons at systole for Control and HCM and for TPSs and Fully Euclidean methods are depicted. In Fig. 22 is evident that, independently from the method (TPSs or Fully Euclidean) and from the cohort under study (Control or HCM) epicardium has always a larger non affine component while the endocardium has always a larger deviatoric component.

Following the logic exposed above, we found exactly what a qualitative description of the strain line pattern predicts: independently from healthy/pathological status and from the use of the three different methods, we found that epicardium presents a non affine component (probably related to the torsion) always significantly larger (via ANOVA) than in endocardium, while the latter

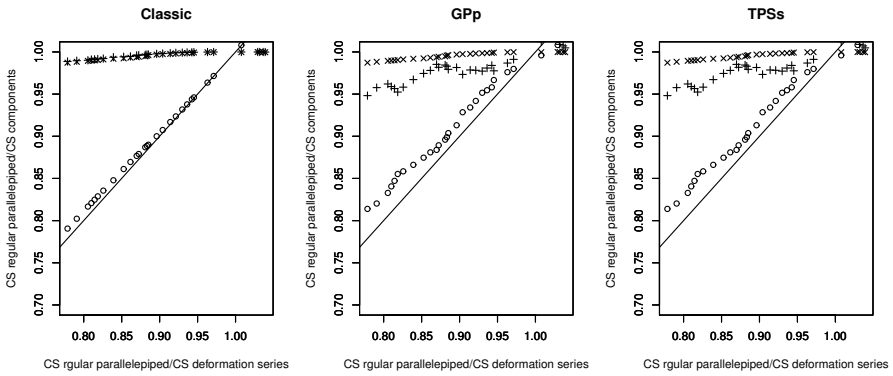

Figure 19: Ratio betwen the CS of the source (regular parallelepiped) and that of the shape associated to any individual component (spherical, deviatoric or non affine) plotted vs. the ratio between source' m-Volume and and that of its actual deformed state; "o" symbol indicates the spherical component; "x" symbol indicates the non affine component; "+" symbol indicates the deviatoric component.

shows a deviatoric component (here an aspect ratio change) always larger than in epicardium. Confirming quantitatively this prediction represents a very important result for the understanding of left ventricle mechanics and in general for cardiac functioning.

This has been depicted in Fig. 23 and 24 where PSL have been mapped on the deformation occurring in systole starting from diastole for the mean shape of Control and HCM respectively. PSL have been computed on total deformation and on the individual components. It can be noted that the deviatoric component of epicardium and endocardium differ visibly as the former has a more oblique PSL indicating smaller affine component while the latter shows a quasi-circumferential pattern proper of an aspect ratio change as predicted by Continuum Mechanics. Moreover, it can be appreciated that the PSL pattern of the total deformation of endocardium is very similar to that found in the deviatoric component, while it is more similar to the non affine one for the epicardium.

7. Conclusions

We have presented in this study a detailed survey on how to define and quantify different components of deformation between shapes represented by homologous landmarks. We did this in the context of cardiological data coming from 3D STE, a gold standard technology for following LV deformation in time. However, we first presented results of three main strategies ("Fully Euclidean" "GPp", "TPSs") coming from simluated/controlled experiments in order to depict the meaning of the three methods and their deep differences when evaluated in known deformative processes. This allowed to appreciate the distinction of different size measures: CS and m-Volume. While the former is widely used in GM, the latter is more used in Continuum Mechanics and has

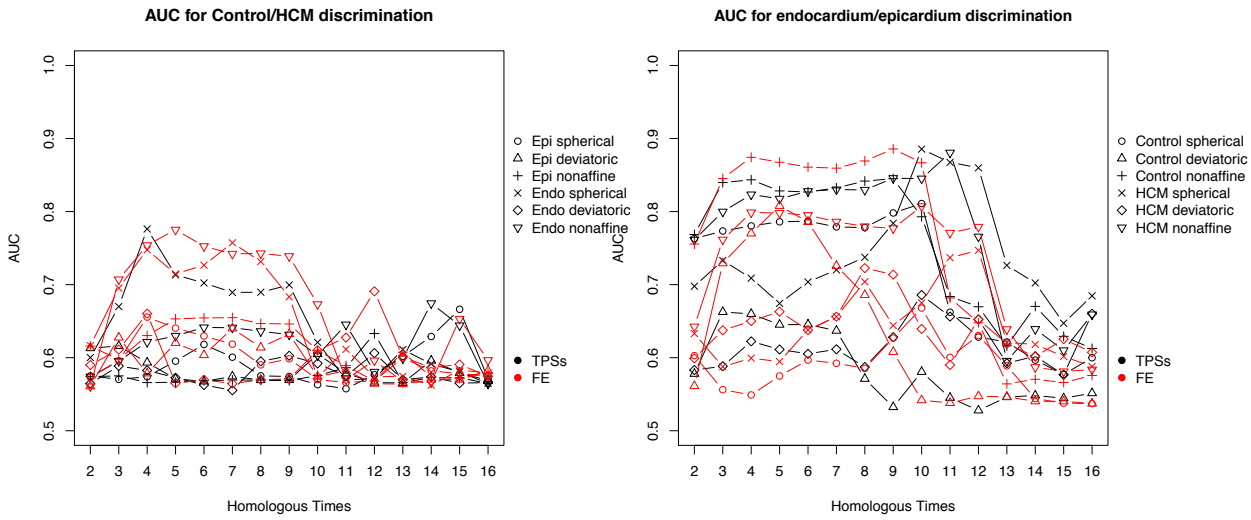

Figure 20: SVM based AUC results, after 1000 randomizations, for Control/HCM (left) and epicardium/endocardium (right) recognition at all homologous times for individual fractions.

a more physical meaning in comparison to CS. The use of CS as size measure is often motivated upon the fact that this is "uncorrelated with shape". However this is strictly dependent on the distribution of shape data around their mean. In fact, quoting (Bookstein, 1989b) "the space of size variables is the set of all distances between landmark points in pairs. If the joint distribution of these distances is that given by variation of each landmark point around a true mean location by small, independent, identically distributed circular normal errors, then the variable G uncorrelated with all distance-ratios is centroid size, square-root of the sum of squares of distances of all the points from their center' of gravity". Being "uncorrelated" means that no allometric effect is present when relating shape with size. However, the centroid size computation is totally agnostic relatively to the question of isometric or allometric shape change. The size computation per se has no information about landmarks distribution and the assumption of "identically distributed circular normal errors" is completely platonic with respect to real data. Consequently, CS is not intrinsically a shape independent size measure. Thus, there is no "perfect" size index and the most appropriate measure for a particular study will depend on particular forms investigated and on the purposes of the study. In the clinical case of LV deformation the m-Volume is the natural, universally used size measure and we proposed two methods ("GPp" and "TPSs") that consider it as the size variable. As a consequence the decomposition of deformation should follow the corresponding size measure adopted as size index.

Our three strategies can be adapted to specific collections of forms that, in each particular cases, could require different methods. We also have shown that decomposing the total LV' deformation allowed to achieve an important corroboration of Continuum Mechanics prediction

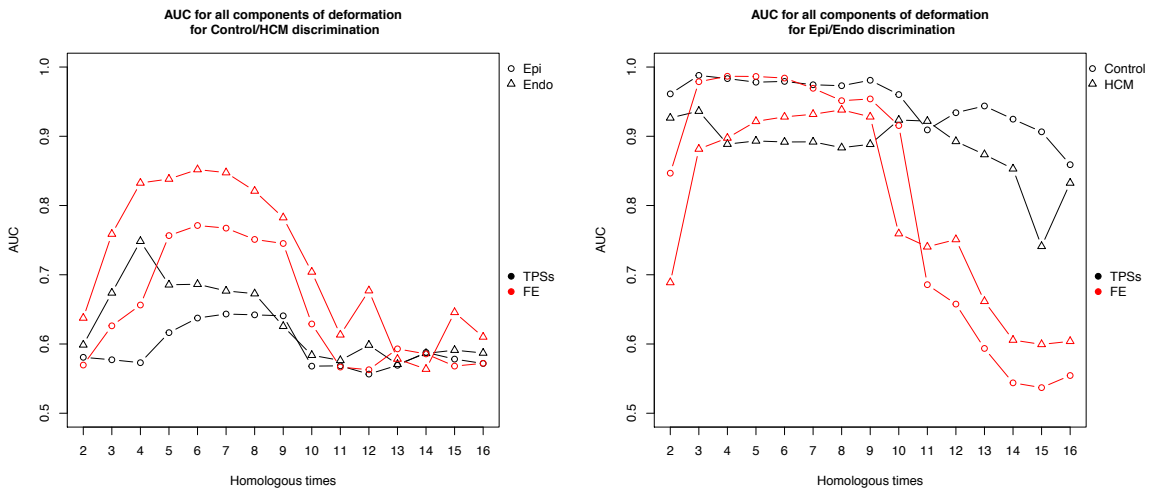

Figure 21: SVM based AUC results, after 1000 randomizations, for Control/HCM (left) and epicardium/endocardium (right) recognition at all homologous times for fraction's decompositions combined together.

about the differential modes of shape changes of epicardial and endocardial layers.

References

Bookstein, F. L. 1989. Principal Warps: Thin-Plate Splines and the Decomposition of Deformations. Journal IEEE Transactions on Pattern Analysis and Machine Intelligence archive, Vol.11 Issue 6: 567-585.

Bookstein, F. L. 1989. 'Size and Shape": A Comment on Semantics. 1989. Syst. Zool., 38(2): 173-180

Bookstein, F. L. 1997. Two shape metrics for biomedical outline data: Bending energy, Procrustes distance, and the biometrical modeling of shape phenomena, Proceedings of 1997 International Conference on Shape Modeling and Applications.

Bookstein, F. L. and W. D. K. Green. 1993. A feature space for edgels in images with landmarks. J. Math. Imaging and Vision 3, 231-261.

Bookstein, F. L. 1996. Landmark methods for forms without landmarks: localizing group differences in outline shape. Conference: Mathematical Methods in Biomedical Image Analysis, 1996. Proceedings of the Workshop.

Bookstein, F. L. 1996, Biometrics, biomathematics, and the morphometric synthesis. Bulletin of Mathematical Biology 58:313-365.

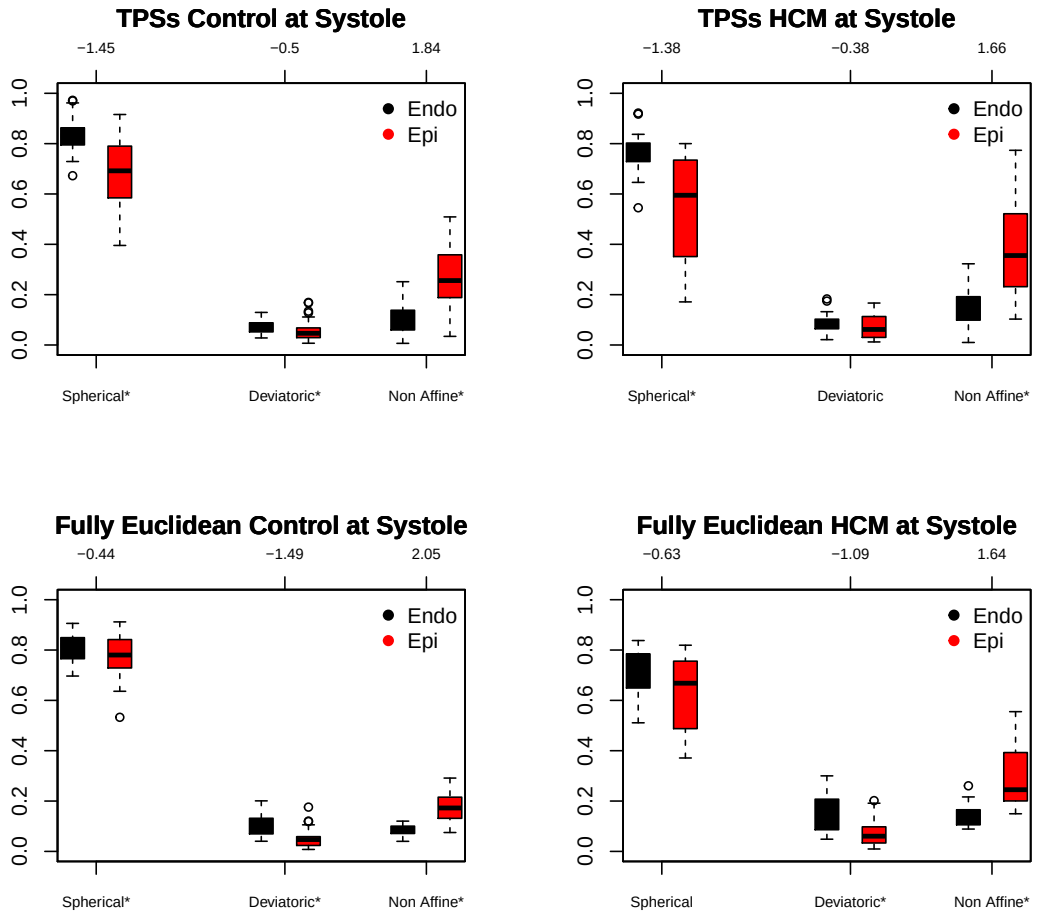

Figure 22: Boxplots at homologous time corresponding to systo-diasolic difference for the Fully Euclidean and TPSs methods for epicardium/endocardium comparison for the three fractions for Control and HCM separately. Asterisks in bottom x-axis indicate significance under ANOVA. Values in top x-axis indicate Cohen'd effectt size.

Bookstein F.L. 1997a. Procrustes Distance, bending Energy and the biometrical modelling of shape phenomena. Int. J. Shape Modell. 3: 17-38.

Bookstein F.L. 1997b. Landmark methods for forms without landmarks: morphometrics of group differences in outline shape. Medical Image Analysis 10(3):225-243

Bookstein F.L 1998. Singularities and the Features of Deformation Grids. Proceedings. Workshop on Biomedical Image Analysis, Santa Barbara (CA). 26-27 Jun 1998: 46-55

Fred L. Bookstein. 1999. Linear Methods for Nonlinear Maps. Brain Warping, 157-181.

Bookstein, F.L. 2000. Creases as local features of deformation grids Medical Image Analysis 4 (2000) 93-110

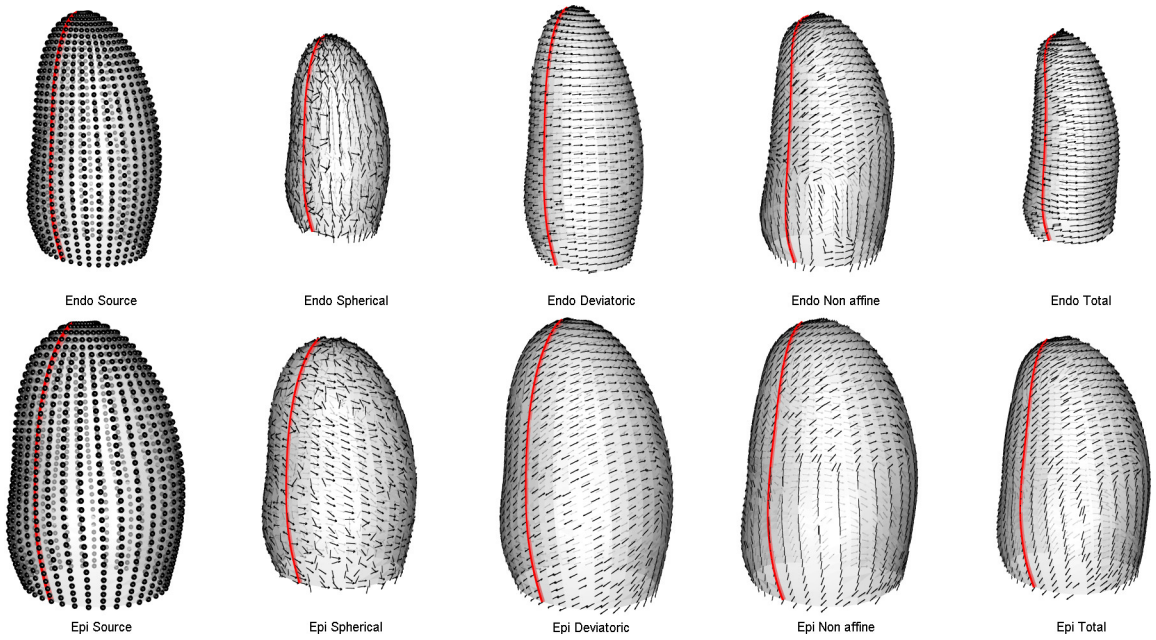

Figure 23: PSL computed on individual components of deformation and on the total deformation at the homologous time corresponding to systo-diasolic difference using the mean shapes of diastole and systole of the Control sample.

Pokrass J., M. Bronstein A., Bronstein M. M., Partial shape matching without point-wise correspondence, Numerical Mathematics: Theory, Methods and Applications (NM-TMA), Vol. 6/1, pp. 223, 2013

Dryden, I.L., Mardia, K.V. 2016 Statistical Shape Analysis 2nd edition, Wiley.

Dryden, I.L., Mardia, K.V. 1998 Statistical Shape Analysis, Wiley.

A. Evangelista, P. Nardinocchi, P.E. Puddu, C. Torromeo, L. Teresi, V. Varano. Torsion of the human left ventricle: experimental analysis and computational modelling. Progress in Biophysics & Molecular Biology, 107 (1), pp. 112-121 (2011), ISSN: 0079-6107

A. Evangelista, S. Gabriele, P. Nardinocchi, P. Piras, P.E. Puddu, L. Teresi, C. Torromeo, V. Varano. Non-invasive assessment of functional strain lines in the real human left ventricle via speckle tracking echocardiography. Journal of Biomechanics, 48, pp. 465471 (2015). doi: 10.1016/j.jbiomech.2014.12.028

Gabriele, S., Teresi, L., Varano, V., Evangelista, A., Nardinocchi, P., Puddu, P.E., Torromeo, C., 2014. A comparative analysis of the strain-line pattern in the human left ventricle: experiments vs modelling. Comput. Methods Biomech. Biomed. Eng. Imaging Visual.

Gabriele, S., Nardinocchi, P., Varano, V., 2015. Evaluation of the strain-line patterns in a human left ventricle: a simulation study. Comput. Methods Biomech. Biomed. Eng. 18 (7), 790-798.

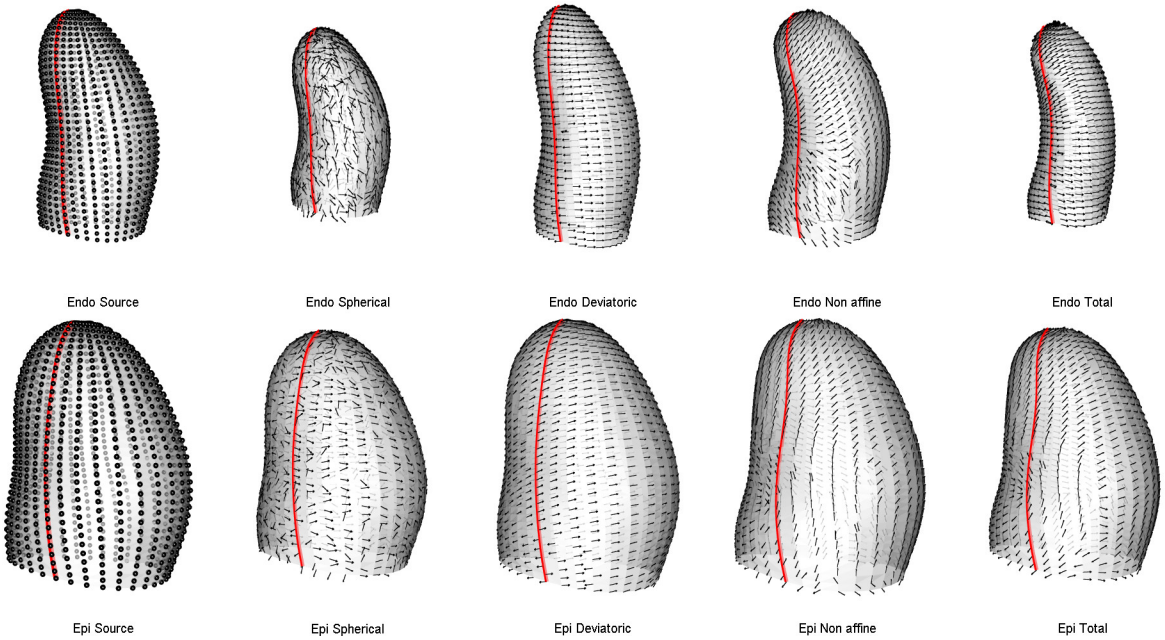

Figure 24: PSL computed on individual components of deformation and on the total deformation at the homologous time corresponding to systo-diasolic difference using the mean shapes of diastole and systole of the HCM sample.

Green, P. J. and Silverman, B. W. 1994. Non-parametric Regression and Generalized Linear Models: A Roughness Penalty Approach. Chapman and Hall, London.

A. Madeo, P. Piras, F. Re, S. Gabriele, P. Nardinocchi, L. Teresi, C. Torromeo, C. Chialastri, M. Schiariti, G. Giura, A. Evangelista, T. Dominici, V. Varano, E. Zachara, P. E. Puddu. A new 4D trajectory-based approach unveils abnormal LV revolution dynamics in hypertrophic cardiomyopathy. PLOS ONE, (2015). doi: 10.1371/journal.pone.0122376

Miller M. I., Qiu A., 2009. The emerging discipline of Computational Functional Anatomy. Neuroimage 45 516-539

Miller, M. I., Mori, S., Qiu, A., Zhang, J., and Ceritoglu, C. 2013. Advanced cost functions for image registration for automated image analysis: Multi- channel, hypertemplate, and atlas with built-in variability. Patent n. US 8600131 B2.

M. Miller, L. Younes and A. Trouvé. Diffeomorphometry and geodesic positioning systems for human anatomy. Technology 02,(36), 2014.

M. Miller, L. Younes and A. Trouvé. Hamiltonian Systems in Computational Anatomy: 100 Years since D'Arcy Thompson. Annual Review of Biomedical Engineering 17 , 2015

P. Nardinocchi, L. Teresi, V. Varano. Strain Induced Shape Formation in Cylindrical Tubes. Journal of the Mechanics and Physics of Solids, 60, n. 8, pp. 1420-1431(2012).

Piras P., Torromeo C., Evangelista A., Gabriele S., Esposito G., Nardinocchi P., Teresi L., Madeo A., Schiariti M., Varano V., Puddu P.E. (2017). Homeostatic Left Heart integration and disintegration links atrio-ventricular covariation?s dyshomeostasis in Hypertrophic Cardiomyopathy. Scientific Reports 2017 Jul 24;7(1):6257. doi: 10.1038/s41598-017-06189-w.

Rohlf, F.J. & Bookstein, F.L. 2003. Computing the uniform component of shape variation. Systematic Biology , 52: 66-69.

Sengupta, P.P.,Tajik ,A.J.,Chandrasekaran, K.,Khandheria,B.K.,2009. Twist mechanics of the left ventricle: principles and application. J.Am.Coll.Cardiol.Imaging 1, 366-376.

Varano V., Gabriele S., Teresi L., Dryden I., Puddu P.E., Torromeo C., Piras P. 2017. The TPS Direct Transport: A New Method for Transporting Deformations in the Size-and-Shape Space. International Journal of Computer Vision. doi:10.1007/s11263-017-1031-9.

Younes L. 2010 Shapes and diffeomorphisms, in Applied Mathematical Sciences, vol. 171, Berlin, Springer–Verlag.

Appendix 1: Projectors features

We can proof that $X\Gamma_{21}$ and $\Phi\Gamma_{11}$ are two complementary projectors (idempotents), in fact:

$$
\begin{aligned}
(X\Gamma_{21})(X\Gamma_{21}) &= X\left(X^T\Phi^{-1}X\right)^{-1}X^T\Phi^{-1}X\left(X^T\Phi^{-1}X\right)^{-1}X^T\Phi^{-1} = X\Gamma_{21} && (7.1)\\
(\Phi\Gamma_{11})(\Phi\Gamma_{11}) &= (I - X\Gamma_{21})(I - X\Gamma_{21}) = I - 2X\Gamma_{21} + (X\Gamma_{21})(X\Gamma_{21}) = \Phi\Gamma_{11} && (7.2)\\
(X\Gamma_{21})(\Phi\Gamma_{11}) &= (\Phi\Gamma_{11})(X\Gamma_{21}) = (I - X\Gamma_{21})X\Gamma_{21} = X\Gamma_{21} - X\Gamma_{21} = 0 && (7.3)
\end{aligned}
$$

We can also check if the two components are orthogonal under the Euclidean metric:

$$
\begin{aligned}
V_u \cdot V_{nu} &= \mathrm{Tr}\left(V_u^T V_{nu}\right) = \mathrm{Tr}\left(V^T\Gamma_{21}^T X^T\Phi\Gamma_{11}V\right) = \mathrm{Tr}\left(V^T\Gamma_{21}^T X^T(I - X\Gamma_{21})V\right)\\
&= \mathrm{Tr}\left(V^T(\Gamma_{21}^T X^T - \Gamma_{21}^T X^T X\Gamma_{21})V\right)\\
&= \mathrm{Tr}\left(V^T\left(\Phi^{-1}X(X^T\Phi^{-1}X)^{-1}X^T - \Phi^{-1}X(X^T\Phi^{-1}X)^{-1}X^T X(X^T\Phi^{-1}X)^{-1}X^T\Phi^{-1})V\right)\right.\\
&= 0 \Leftrightarrow \Phi = I && (7.4)
\end{aligned}
$$

Only the pseudo inverse based decomposition is compatible with the Euclidean metric.